Spherical near-field antenna measurements — **Source link** ↗

J. E. Hansen

Published on: 01 Jan 1988

Topics: Antenna (radio) and Near and far field

Related papers:

- An overview of near-field antenna measurements

- Representation of electromagnetic fields over arbitrary surfaces by a finite and nonredundant number of samples

- Time-harmonic electromagnetic fields

- Near-field to near/far-field transformation for arbitrary near-field geometry utilizing an equivalent electric current and MoM

- On the spatial bandwidth of scattered fields

SPHERICAL NEAR FIELD ANTENNA MEASUREMENTS

A THESIS SUBMITTED TO
THE GRADUATE SCHOOL OF NATURAL AND APPLIED SCIENCES
OF
MIDDLE EAST TECHNICAL UNIVERSITY

BY

HÜSNÜ DOĞAN KILIÇ

IN PARTIAL FULFILLMENT OF THE REQUIREMENTS
FOR
THE DEGREE OF MASTER OF SCIENCE
IN
ELECTRICAL AND ELECTRONICS ENGINEERING

SEPTEMBER 2019

Approval of the thesis:

SPHERICAL NEAR FIELD ANTENNA MEASUREMENTS

submitted by **HÜSNÜ DOĞAN KILIÇ** in partial fulfillment of the requirements for the degree of **Master of Science in Electrical and Electronics Engineering Department, Middle East Technical University** by,

Prof. Dr. Halil Kalıpçılar
Dean, Graduate School of **Natural and Applied Sciences**　　　　_____

Prof. Dr. İlkay Ulusoy
Head of Department, **Electrical and Electronics Eng.**　　　　_____

Prof. Dr. Seyit Sencer Koç
Supervisor, **Electrical and Electronics Eng., METU**　　　　_____

Examining Committee Members:

Prof. Dr. Gülbin Dural
Electrical and Electronics Engineering, METU　　　　_____

Prof. Dr. Seyit Sencer Koç
Electrical and Electronics Eng., METU　　　　_____

Prof. Dr. Vakur Behçet Ertürk
Electrical and Electronics Engineering, Bilkent University　　　　_____

Assoc. Prof. Dr. Lale Alatan
Electrical and Electronics Engineering, METU　　　　_____

Prof. Dr. Asım Egemen Yılmaz
Electrical and Electronics Engineering, Ankara University　　　　_____

Date: 09.09.2019

I hereby declare that all information in this document has been obtained and presented in accordance with academic rules and ethical conduct. I also declare that, as required by these rules and conduct, I have fully cited and referenced all material and results that are not original to this work.

Name, Surname: Hüsnü Doğan Kılıç

Signature:

ABSTRACT

SPHERICAL NEAR FIELD ANTENNA MEASUREMENTS

Kılıç, Hüsnü Doğan
Master of Science, Electrical and Electronics Engineering
Supervisor: Prof. Dr. Seyit Sencer Koç

September 2019, 60 pages

Accurate determination of the antenna characteristics is one of the key subjects where different methods have been developed for this purpose. When advantages and facilities of these methods are considered, near field measurements have come forward especially in recent years. In this thesis, one of these methods which is referred to as spherical near field measurement method, has been studied. First, wave expansion in the spherical coordinates is introduced. This enables expressing the field as summation of modes which are composed of vector wave functions and coefficients of these functions. It is shown that by obtaining coefficients for measurement distance, field can be obtained at any other distance with these coefficients. However, test setup of an antenna is composed of receiver and transmitter such that one of them is antenna under test and other is measurement antenna which is usually called the probe. Hence, probe effects on the measurement must also be included for accurate results. Initially, Lorentz's Reciprocity Theorem had been used for this purpose. Then scattering matrix theory has been more commonly used. In this thesis study, scattering matrix theory is explained and generation of transmission formula with the probe compensation is presented. Different numerical integration techniques are used in order to calculate wave coefficients and comparisons are given. Eventually, tests with the theoretical data and results of measured antennas are performed and results are discussed.

ÖZ

KÜRESEL YAKIN ALAN ANTEN ÖLÇÜMLERİ

Kılıç, Hüsnü Doğan
Yüksek Lisans, Elektrik ve Elektronik Mühendisliği
Tez Danışmanı: Prof. Dr. Seyit Sencer Koç

Eylül 2019, 60 sayfa

Anten karakteristiğinin doğru bir şekilde belirlenmesi büyük öneme sahip konulardan biridir ki bu amaç doğrultusunda farklı metotodlar geliştirilmiştir. Bu metotların avantajları ve kolaylıkları düşünüldüğü zaman, özellikle son yıllarda yakın alan ölçümleri öne çıkmaktadır. Bu tezde, bu metotlardan biri olan küresel yakın alan ölçüm metodu çalışılmıştır. İlk olarak küresel koordinatlarda dalga açılımı gösterilmiştir. Bu, alanı vektör dalga fonksiyonlarından ve bu fonksiyonların katsayılarından oluşan modların toplamı olarak ifade etmeyi sağlar. Ölçüm yapılan mesafede katsayıları elde ederek, bu katsayılarla alanın herhangi bir mesafede bulunabileceği gösterilmiştir. Fakat bir antenin test kurulumu alıcı ve vericiden oluşur, öyle ki bunlardan biri test altındaki anten, diğeri ise genellikle ölçüm ucu olarak adlandırılan ölçüm antenidir. Bu nedenle, doğru sonuçlar için ölçüm ucunun ölçüme etkileri de dahil edilmelidir. Bu amaç için ilk olarak Lorentz Karşılıklılık Teoremi kullanılmıştır. Sonrasında, saçılım matris teorisi yaygın olarak kullanılmıştır. Bu tez çalışmasında saçılım matris teorisi açıklanmış ve ölçüm ucunun etkilerini telafi ederek iletim formülü türetimi gösterilmiştir. Dalga katsayılarını hesaplamak için farklı nümerik integral teknikleri kullanılmış ve karşılaştırmalar yapılmıştır. Son olarak, teorik veriler ve ölçülen antenlerin sonuçları kullanılarak testler yapılmış ve sonuçlar irdelenmiştir.

Anahtar Kelimeler: Yakın Alandan Uzak Alana Dönüşüm, Küresel Dalga Açılımı, Anten Saçılım Matris Teorisi, İletim Formülü, Nümerik İntegral Alma

To my father, my mother, my fiancée and my niece Zeynep

ACKNOWLEDGEMENTS

TABLE OF CONTENTS

LIST OF TABLES

TABLES

LIST OF FIGURES

FIGURES

LIST OF ABBREVIATIONS

ABBREVIATIONS

AUT	Antenna Under Test
SNIFT	Spherical Near Field Far Field Transformation Code
FF	Far Field
NF	Near Field
DFT	Discrete Fourier Transform
IDFT	Inverse Discrete Fourier Transform
FFT	Fast Fourier Transform

LIST OF SYMBOLS

SYMBOLS

ε Permittivity

μ Permeability

k Propagation Constant

Γ Reflection Coefficient

η Wave Impedance

CHAPTER 1

INTRODUCTION

An antenna is a structure that receives and transmits electromagnetic signals. With the high pace of development in technology, wireless communication have become one of the most critical subjects all over the world and antennas are the key devices in this field. Developments in technology have required more efficient, more accurate and faster measurement solutions for antenna testing. Antennas are generally used to transmit information to far distances so most of the time performance criteria of an antenna is described for the far field region. Hence, first solution for the antenna testing was measuring the antenna at sufficiently far distances. Far field antenna measurement technique has been used over the years. However, with the advance and increasing usage of technology in the area of communication, defense and health, designing lots of different types of antennas and producing plenty amount of them have been essential. When this was the case, drawbacks of the far field antenna measurement became more apparent. First of all; depending on the antenna type and dimensions, required range for the far field may be too much so establishing the measurement region may be troublesome and costly. If the measurement area is outdoor region that was usually the case, then measurements are affected from the weather conditions which sometimes may not allow to make measurements. In addition to these, eliminating effects from the ground and surrounding objects can be impossible. Measurement time can be too much especially for large distances. Transportation and mounting may be problematic for large antennas. Because of these reasons, researchers sought for ways of determining far field properties from the measurement in the near field region. Basically three techniques have aroused which are pattern measurement with focused antenna, compact range and transformation of near field measurement data to obtain far field pattern [1]. In the first technique,

1

antenna is focused to near field region and measurement is performed. In the second technique, approximate uniform plane wave is created using a reflector and so measurement can be taken with far field conditions. In the last method, measurement is done in the near field and far field pattern is calculated using transformation.

Historically, researches on the near field antenna measurements started around 1950's [2]. Around 1950, Barrett and Barnes from the Air Force Cambridge Research Center started to investigate near field by using an antenna scanner [3]. The aim was not to calculate the far field since the theory was not established at that time. Then, Woonton [4] studied the relation between the induced voltage on the probe with electric field strength by making near field measurements. Richmond and Tice [5], [6] compared the near and far field pattern with experiments in 1955. Some researchers made experiments using particular line sources. Gamara [7] compared near field and far field patterns for particular line sources by taking measurement directly in the far field distance and calculating far field pattern from the measurements done in the near field in 1960. Brown and Jull [8] used cylindrical wave expansion in two dimensions and verified their work experimentally. Besides, they proposed a method for probe correction in 1961. However, complete probe compensation method was given by Kern in 1963 [9]. He used plane wave expansion method with scattering matrix theory of the antenna. After planar scanning solution, three dimensional cylindrical probe compensated method was improved by Leach and Paris in 1973 [10]. The probe correction with the spherical wave expansion method which enabled the spherical scanning was derived by Jensen in 1970 [11]. Works of Wacker's in 1974 [12] and 1975 [13] with work of Jensen in 1975 [14] showed implementation of the theory can be put into practice. Lots of studies and implementations have been performed but the complete algorithm for the spherical near field measurement with probe correction was given by Larsen in 1977 [15].

In this thesis, spherical near field measurement is discussed. First, spherical wave theory is explained and determination of the far field from the near field without probe compensation is given. Afterwards, transformation for the probe corrected case is

explained by giving the scattering matrix definition of the antenna. Discussions about truncation value of modes and different numerical integration techniques are also included. Finally, applications and results for the theoretical data and measured antennas using the developed algorithm is presented.

CHAPTER 2

SPHERICAL WAVE EXPANSION

2.1. Spherical Vector Wave Functions

Maxwell's equations of the electromagnetic field for linear, isotropic and homogenous medium with taking time dependence as $e^{-i\omega t}$ are

$$\overline{\nabla} \times \vec{E} = i\omega\mu\vec{H} - \vec{M} \qquad (2.1)$$

$$\overline{\nabla} \times \vec{H} = -i\omega\varepsilon\vec{E} + \vec{J} \qquad (2.2)$$

where $\vec{E}$ and $\vec{H}$ are electric and magnetic field vectors, $\vec{J}$ and $\vec{M}$ are electric and magnetic current density vectors, ε and μ are permittivity and permeability, respectively. When curl of each sides of the equations are taken with assuming source free region, it is concluded that both electric and magnetic field vectors satisfy the vector differential equation

$$\overline{\nabla} \times \overline{\nabla} \times \vec{F} - k^2\vec{F} = 0 \qquad (2.3)$$

where $k = \omega\sqrt{\mu\varepsilon} = 2\pi/\lambda$ is the propagation constant and $\vec{F}$ is an arbitrary vector. As a consequence, each component of the field vectors satisfies the scalar Helmholtz equation. Let f be a solution of the scalar Helmholtz equation

$$(\nabla^2 + k^2)f = 0 \qquad (2.4)$$

Now the following independent vector solutions satisfy equation (2.3).

$$\vec{M} = \overline{\nabla}f \times \vec{r} \qquad (2.5)$$

$$\vec{N} = \frac{1}{k}\overline{\nabla} \times \vec{M} \qquad (2.6)$$

As it is understood from equations (2.5) and (2.6), $\vec{M}$ and $\vec{N}$ are related with curl operator and they are solenoidal functions. Then, they can be used in order to express source free electromagnetic fields ($\vec{E},\vec{H}$).

Note also that vector $\vec{L}$ appears when divergence of the field is not zero which is the case where sources are included.

$$\vec{L} = \nabla\psi \tag{2.7}$$

However; it is not used in this work because solutions are determined for source free regions.

The function f for the spherical waves is obtained using separation of variables as given in [16] by Stratton,

$$f_{\substack{e \\ o}mn}^{(c)}(r,\theta,\emptyset) = z_n^{(c)}(kr)P_n^m(\cos\theta)\frac{\cos}{\sin}m\emptyset \tag{2.8}$$

with $n = 1, 2, 3 \dots$ and $m = 0, 1, 2, \dots, n$. e and o subscripts in the equation describes even and odd part of the $\emptyset$ dependence of the trigonometric function. $P_n^m(\cos\theta)$ function is the associated Legendre function and $z_n^{(c)}(kr)$ is one of the followings with specified c index

$$z_n^{(1)}(kr) = j_n(kr) \text{ (spherical Bessel function)} \tag{2.9}$$

$$z_n^{(2)}(kr) = n_n(kr) \text{ (spherical Neumann function)} \tag{2.10}$$

$$z_n^{(3)}(kr) = h_n^{(1)}(kr) = j_n(kr) + in_n(kr) \text{ (spherical Hankel function of first kind)} \tag{2.11}$$

$$z_n^{(4)}(kr) = h_n^{(2)}(kr) = j_n(kr) - in_n(kr) \text{ (spherical Hankel function of second kind)} \tag{2.12}$$

where Bessel function and Neumann functions represent the standing waves and first kind of Hankel function and second kind of Hankel function represent outward and inward travelling waves, respectively.

By substituting function f in equation (2.8) into equations (2.5) and (2.6) and following notations and definitions in [17], spherical vector wave functions are obtained as;

$$\vec{M}_{\substack{e \\ o mn}}^{(c)}(r, \theta, \emptyset) = \mp z_n^{(c)}(kr) \frac{mP_n^m(\cos\theta)}{\sin\theta} \frac{\cos}{\sin} m\emptyset \,\hat{\theta}$$
$$- z_n^{(c)}(kr) \frac{dP_n^m(\cos\theta)}{d\theta} \frac{\cos}{\sin} m\emptyset \,\hat{\emptyset} \tag{2.13}$$

$$\vec{N}_{\substack{e \\ o mn}}^{(c)}(r, \theta, \emptyset) = \frac{n(n+1)}{kr} z_n^{(c)}(kr) P_n^m(\cos\theta) \frac{\cos}{\sin} m\emptyset \,\hat{r}$$
$$+ \frac{1}{r}\frac{d}{dr}\{rz_n^{(c)}(kr)\} \frac{dP_n^m(\cos\theta)}{d\theta} \frac{\cos}{\sin} m\emptyset \,\hat{\theta} \tag{2.14}$$
$$\mp \frac{1}{r}\frac{d}{dr}\{rz_n^{(c)}(kr)\} \frac{mP_n^m(\cos\theta)}{\sin\theta} \frac{\cos}{\sin} m\emptyset \,\hat{\emptyset}$$

In order to obtain more compact form and for computational convenience, instead of even and odd parts, only $e^{im\emptyset}$ will be used as done by Jensen [11] and Jones [18]. In addition; computation for associated Legendre function is done with power normalized form. This form enables to compute vector wave functions with high values of n and m. By inserting these changes and defining $\left(-\frac{m}{|m|}\right)^m = 1$ for $m = 0$, we get the final forms of spherical vector wave functions as

$$\vec{M}_{mn}^{(c)}(r, \theta, \emptyset) = \frac{1}{\sqrt{2\pi n(n+1)}}\left(-\frac{m}{|m|}\right)^m \left\{ \frac{im\bar{P}_n^{|m|}(\cos\theta)}{\sin\theta}\hat{\theta} \right.$$
$$\left. - \frac{d\bar{P}_n^{|m|}(\cos\theta)}{d\theta}\hat{\emptyset} \right\} z_n^{(c)}(kr) e^{im\emptyset} \tag{2.15}$$

$$\vec{N}_{mn}^{(c)}(r, \theta, \emptyset)$$
$$= \frac{1}{\sqrt{2\pi n(n+1)}}\left(-\frac{m}{|m|}\right)^m \left\{ \frac{n(n+1)}{r} z_n^{(c)}(kr)\bar{P}_n^{|m|}(\cos\theta)\hat{r} \right.$$
$$+ \frac{1}{r}\frac{d}{dr}\{rz_n^{(c)}(kr)\} \frac{d\bar{P}_n^{|m|}(\cos\theta)}{d\theta}\hat{\theta} \tag{2.16}$$
$$\left. + \frac{1}{r}\frac{d}{dr}\{rz_n^{(c)}(kr)\} \frac{im\bar{P}_n^{|m|}(\cos\theta)}{\sin\theta}\hat{\emptyset} \right\} e^{im\emptyset}$$

where $n = 1, 2, 3 \dots$ and $m = -n, -n + 1, \dots, n - 1, n$. $\bar{P}_n^m$ is the normalized associated Legendre function which is defined as

$$\bar{P}_n^m = \sqrt{\frac{2n + 1}{2} \frac{(n - m)!}{(n + m)!}} \, P_n^m \qquad (2.17)$$

Now, the electric and magnetic fields for the source free region can be written as a weighted sum of spherical vector wave functions

$$\vec{E}(r, \theta, \emptyset) = \frac{k}{\sqrt{\eta}} \sum_{n=1}^{\infty} \sum_{m=-n}^{n} a_{mn} \vec{M}_{mn}^{(c)} + b_{mn} \vec{N}_{mn}^{(c)} \qquad (2.18)$$

$$\vec{H}(r, \theta, \emptyset) = -ik\sqrt{\eta} \sum_{n=1}^{\infty} \sum_{m=-n}^{n} a_{mn} \vec{N}_{mn}^{(c)} + b_{mn} \vec{M}_{mn}^{(c)} \qquad (2.19)$$

where a_{mn} and b_{mn} are called spherical wave coefficients.

2.1.1. Determination of Far Field Distribution from the Near Field Data

Electric or magnetic fields at any distance from the antenna can now be determined through equations (2.18) and (2.19). As seen from these equations, they are valid for any value of r (distance). However; in the reactive near field region which is the very close proximity of antenna, practical measurement cannot be taken without affecting the radiated field from AUT. Hence, near field measurements must be carried out at the distance which guarantees radiating near field conditions. When wave coefficients are found at measurement distance, they can be used to find field distribution at any distance.

First of all, it must be stated that n in the summation can be truncated at some value N for computational purposes. The reasons of this are discussed in detail in section 4.1. Then by measuring field distributions namely $\vec{E}(r, \theta, \emptyset)$ and $\vec{H}(r, \theta, \emptyset)$ at a value of r_0 and with desired number of θ and $\emptyset$ discrete points, a system of linear equation is obtained from equations (2.18) and (2.19). However, these linear equations generally form a very big system and solving it for each m and n is unpractical. More efficient

way of finding these coefficients can be derived by taking advantage of orthogonality properties of the spherical wave functions. The details of these properties can be found in [17] and [16]. In addition; it is uncovered that in order to find both coefficients, performing measurements at the two tangential field components namely $\hat{\theta}$ and $\widehat{\emptyset}$, is the most efficient method. Briefly; to find a_{mn}, dot product both sides of equation (2.18) with $\vec{M}_{-mn}^{(c)}$ and to find b_{mn} dot product both sides of equation (2.18) with $\vec{N}_{-mn}^{(c)}$ and take the integral on the surface of measurement sphere. By implementing orthogonality properties of vector wave functions, following results are obtained.

$$\int_{\emptyset=0}^{2\pi} \int_{\theta=0}^{\pi} \vec{E}(r_0, \theta, \emptyset) \cdot \vec{M}_{-mn}^{(c)} \sin\theta \, d\theta \, d\emptyset = a_{mn}\{z_n^{(c)}(kr_0)\}^2 \qquad (2.20)$$

$$\int_{\emptyset=0}^{2\pi} \int_{\theta=0}^{\pi} \vec{E}(r_0, \theta, \emptyset) \cdot \vec{N}_{-mn}^{(c)} \sin\theta \, d\theta \, d\emptyset$$
$$= b_{mn}\left\{\frac{1}{r_0}\left(\frac{d}{dr}\left(rz_n^{(c)}(kr)\right)\Big|_{r=r_0}\right)\right\}^2 \qquad (2.21)$$

By solving the integrals on the left hand side of equations (2.20) and (2.21) numerically, wave coefficients are obtained for each m and n. Finally, electric field for the required distance from the antenna (r_1) can be found by putting these coefficients and evaluating $\vec{M}_{mn}^{(c)}$ and $\vec{N}_{mn}^{(c)}$ functions at distance r_1 in equation (2.18).

In this work, $e^{-i\omega t}$ convention is used so in equations (2.20) and (2.21) $c = 3$ corresponds to outgoing wave and $c = 4$ to incoming wave. In the practical measurements of this work, all sources are in the measurement sphere. Hence, outgoing waves will be measured and so $c = 3$ will be used. Note also that radial functions have following asymptotic forms.

$$z_n^{(3)}(kr) = (-i)^{n+1}\frac{e^{ikr}}{kr} \qquad kr \to \infty \qquad (2.22)$$

$$\frac{1}{r}\frac{d}{dr}\left\{rz_n^{(3)}(kr)\right\} = (-i)^n\frac{e^{ikr}}{kr} \qquad kr \to \infty \qquad (2.23)$$

The asymptotic forms of radial functions are used in the evaluation of vector wave functions for the far field.

CHAPTER 3

MEASUREMENT WITH PROBE CORRECTION

In Chapter 2, electric field is obtained by calculating spherical wave coefficients. In these calculations, it is assumed that electric field value at some distance is known. Even if this can be achieved for an antenna with known electric field expression such as Hertz Dipole, in practice; measurements give complex amplitudes of the received signal. Measurement of the received signal is performed with an antenna which is generally called probe. Probe has own characteristics and the effects of it must be extracted to have accurate results. Probe effects can be measured with a calibration procedure and then characterized with probe receiving coefficients. By including these coefficients, the transmission formula can be generated. For the derivation of this formula, first Lorentz Reciprocity Theorem had been used in the literature. Later scattering matrix description of an antenna was built and used in the derivation of the transmission formula. In this chapter, initially scattering matrix description of an antenna is given and then derivation of transmission formula is shown. Note that for this purpose 'Spherical Near-Field Antenna Measurements' book which is edited by J.E. Hansen is followed [17].

3.1. Scattering Matrix Definition of the Antenna

An antenna can be considered as multiport waveguide junction. While the port that is connected to generator and load can be considered as one of the ports, other ports can be considered as radiation ports which can be thought as they are connected to equivalent transmission line for every mode. We define v and w as incoming and outgoing waves complex amplitudes at the generator or load respectively. Also define a and b as complex amplitudes of the incoming and outgoing spherical waves, respectively. Note that these spherical waves are outside the minimum sphere of the

11

antenna and a and b includes the modes of these waves. Then antenna with these wave amplitudes can be depicted as shown in Figure 3.1.
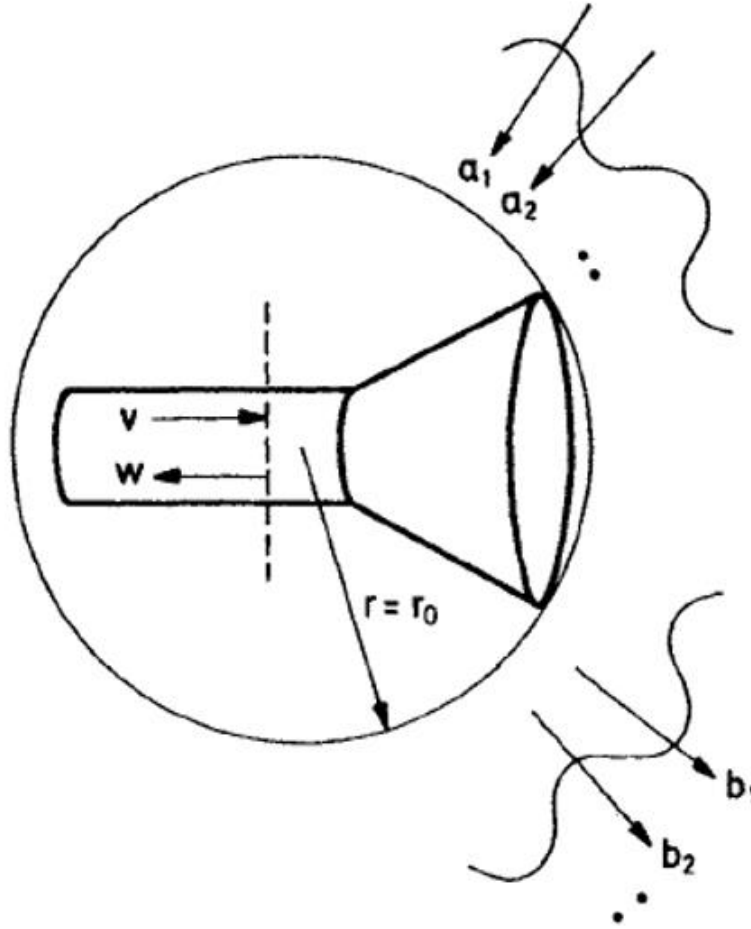
Figure 3.1. Antenna with Scattering Point of View [17]

Because, number of radiated spherical wave modes can be truncated at value N as discussed in section 4.1, the following linear relationship which construct a matrix can be created.

$$\begin{bmatrix} \Gamma & R \\ T & S \end{bmatrix} \begin{bmatrix} v \\ a \end{bmatrix} = \begin{bmatrix} w \\ b \end{bmatrix} \tag{3.1}$$

In equation (3.1); Γ is the antenna reflection coefficient and it is a complex number, R represents the antenna receiving coefficients and it is a $1 \times N$ vector, T represents the antenna transmitting coefficients and it is a $N \times 1$ vector, and S represents the

antenna scattering coefficients and it is a N x N matrix. With expansion of the matrix following equations are obtained.

$$\Gamma v + \sum_{j=1}^{N} R_j a_j = w \qquad (3.2)$$

$$T_i v + \sum_{j=1}^{N} S_{ij} a_j = b_i, \qquad i = 1, 2, \dots, N \qquad (3.3)$$

Consider the antenna in Figure 3.1 as receiver which is connected to a load. Let reflection coefficient between the antenna and load be Γ_l. Then, reflected signal from the antenna is defined as the reflection coefficient multiplied by received signal.

$$v = \Gamma_l w \qquad (3.4)$$

Putting equation (3.4) into equation (3.2) and solving for w gives

$$w = \frac{1}{1 - \Gamma_l \Gamma} \sum_{j=1}^{N} R_j a_j \qquad (3.5)$$

Expression for the receiving signal in terms of scattering matrix parameters is defined by equation (3.5). By the same way transmitting signal can be expressed for the antenna transmitting case but it is not necessary to show it in here because in the following section, probe is used as receiving antenna and transmission formula is written in terms of receiving signals.

3.2. Derivation of the Transmission Formula

Now, consider spherical near field measurement setup that includes an AUT and a probe. For derivation of the transmission formula, AUT is used as transmitting antenna and probe is used as receiving antenna. While AUT is put at the origin of (x, y, z) coordinate system, probe is put at distance A from the AUT origin which it is called as (x', y', z') coordinate system. Note also that probe is always pointing towards the origin of the test antenna throughout the measurement. Test antenna and probe

13

coordinate system with their minimum spheres are shown in Figure 3.2. Minimum sphere is defined as the smallest sphere with center at the origin of the coordinate system and encloses the antenna.
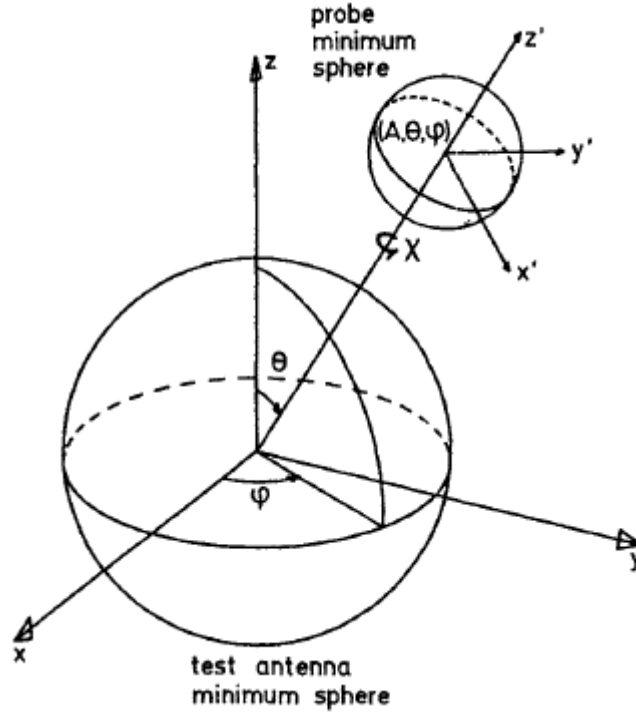
Figure 3.2. Test Antenna and Probe Coordinate Systems [17]

The electric field expression of the radiated field of the transmitting antenna is considered. Before that following notation simplifications are used to reduce the formulation. $\vec{F}_{smn}^{(c)}$ is used instead of vector wave functions $\vec{M}_{mn}^{(c)}$ and $\vec{N}_{mn}^{(c)}$ with $\vec{F}_{1mn}^{(c)} = \vec{M}_{mn}^{(c)}$ and $\vec{F}_{2mn}^{(c)} = \vec{N}_{mn}^{(c)}$. In addition; q_{smn} will be used instead of wave coefficients a_{mn} and b_{mn} with $q_{1mn} = a_{mn}$ and $q_{2mn} = b_{mn}$. Now, the radiated electric field can be expressed as

$$\vec{E}(r,\theta,\emptyset) = \frac{k}{\sqrt{\eta}} \sum_{smn} q_{smn} \vec{F}_{smn}^{(3)}(r,\theta,\emptyset), \qquad r > r_0 \qquad (3.6)$$

where r_0 is the radius of the minimum sphere surround the transmitting antenna. First of all, since this field is received by a probe, it will be expressed in the probe

14

coordinate system which is denoted by primed variables. For this purpose, rotations and translation for the coordinate system are necessary. Mode indices for the transmitting antenna coordinate system is denoted as s, m, n and for the coordinate system of the receiving antenna, σ, μ, ν indices will be used.

Transmitting antenna coordinate system (x, y, z) can be transformed to same orientation with the probe coordinate system (x', y', z') by successive three rotations. As first step, unprimed coordinate system is rotated about its z-axis by an angle $\emptyset_0$ as shown in Figure 3.3.

Figure 3.3. Rotation about z-axis with an angle $\emptyset_0$ [17]

Denoting the new coordinate system by (x_1, y_1, z_1), the vector wave functions in new coordinate system are expressed as

$$\vec{F}_{smn}^{(3)}(r, \theta, \emptyset) = e^{im\emptyset_0} \vec{F}_{smn}^{(3)}(r_1, \theta_1, \emptyset_1), \qquad r_1 > r_0 \qquad (3.7)$$

In the second step, (x_1, y_1, z_1) coordinate system is rotated about the y_1 axis by an angle θ_0 as shown in Figure 3.4.
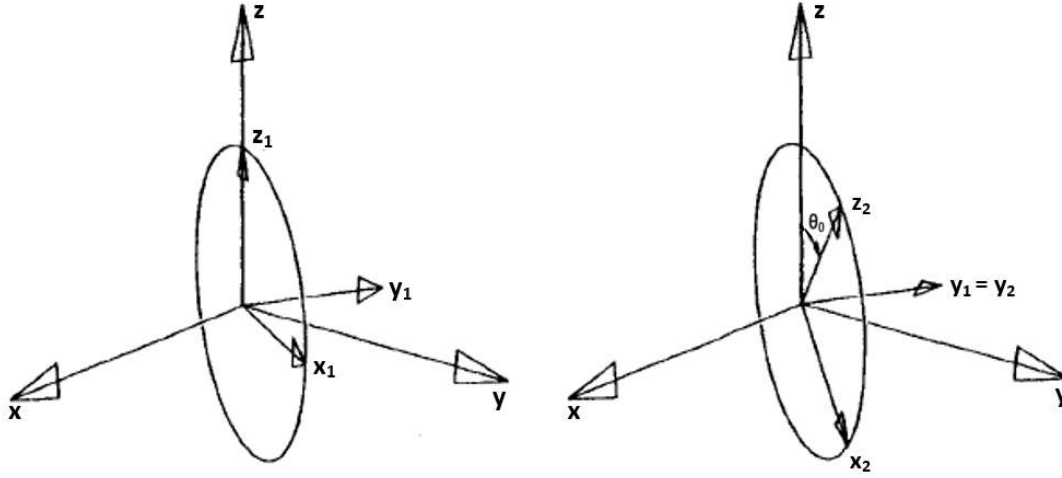
Figure 3.4. Rotation about y_1-axis with an angle θ_0 [17]

Denoting the new coordinate system by (x_2, y_2, z_2), the vector wave functions in new coordinate system are expressed as

$$\vec{F}^{(3)}_{smn}(r_1, \theta_1, \emptyset_1) = \sum_{\mu=-n}^{n} d^n_{\mu m}(\theta_0)\, \vec{F}^{(3)}_{s\mu n}(r_2, \theta_2, \emptyset_2), \qquad r_2 > r_0 \qquad (3.8)$$

where $d^n_{\mu m}(\theta_0)$ are rotation coefficients. Note that z_2 axis becomes parallel to the z' axis as a result of this rotation step.

In the final step of rotation, (x_2, y_2, z_2) coordinate system is rotated with respect to z_2 axis by an angle χ_0 as shown in Figure 3.5. Note that this rotation is required for polarization.
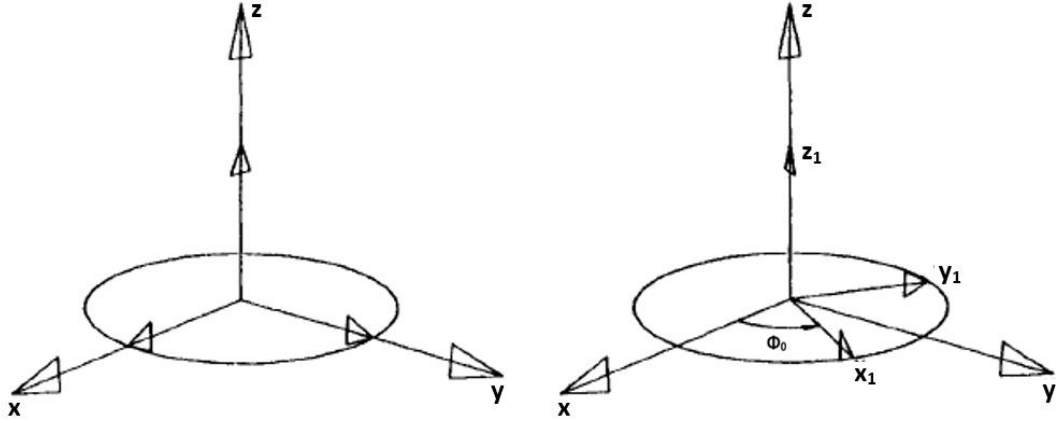
16
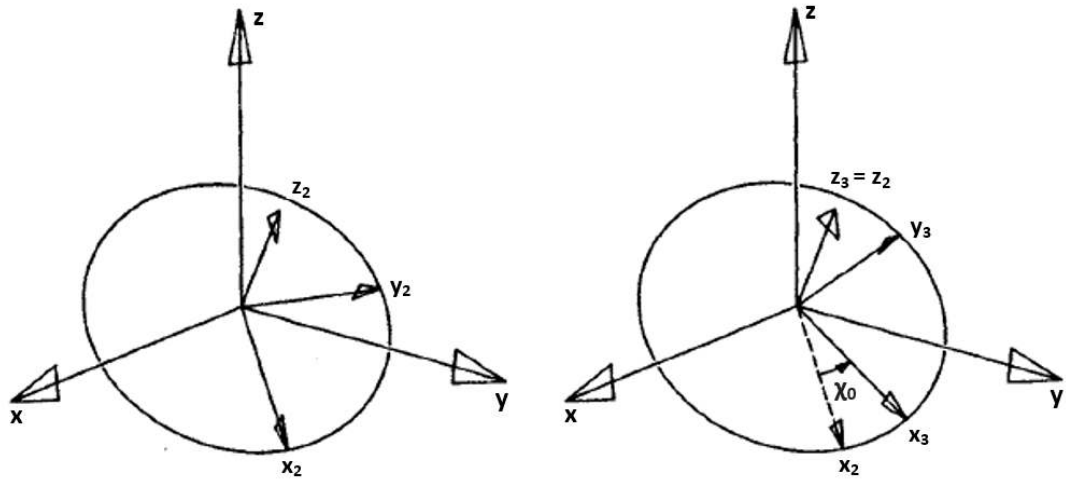
Figure 3.5. Rotation about z_2-axis with an angle χ_0 [17]

Denoting the new coordinate system as (x_3, y_3, z_3), the vector wave functions in new coordinate system are expressed as

$$\vec{F}_{s\mu n}^{(3)}(r_2, \theta_2, \emptyset_2) = e^{i\mu\chi_0}\vec{F}_{s\mu n}^{(3)}(r_3, \theta_3, \emptyset_3), \qquad r_3 > r_0 \qquad (3.9)$$

Rotations about all axes $(\chi, \theta, \emptyset)$ are completed. The coordinate axes of (x_3, y_3, z_3) are now same orientation with the coordinate axes of (x', y', z'). In this situation, $x' = x_3$, $y' = y_3$ and $z' = z_3 + A$ so translation about the z_3 axis by distance A is required to obtain the spherical harmonic expansion of the field radiated by the AUT in the probe coordinate system. Figure 3.6 shows this translation step.
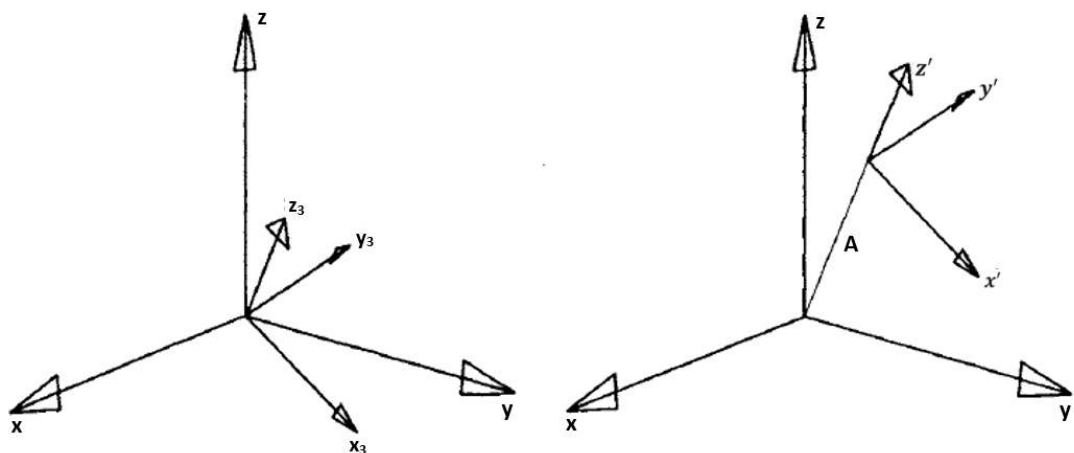
Figure 3.6. Translation in positive direction of z_3-axis [17]

17

With translation step, (x', y', z') coordinate system can be expressed with (x_3, y_3, z_3) coordinate system as given in (3.10).

$$\vec{F}_{s\mu n}^{(3)}(r_3, \theta_3, \emptyset_3) = \sum_{\sigma=1}^{2} \sum_{\substack{\nu=|\mu| \\ \nu \neq 0}}^{N_r} C_{\sigma\mu\nu}^{sn(3)}(kA) \, \vec{F}_{\sigma\mu\nu}^{(1)}(r', \theta', \emptyset'), \tag{3.10}$$

$$r' < A - r_0$$

Equation (3.10) is a finite sum since $r_3 > r_0$ means that only standing waves with $j_n(kr)$ functions occur. Furthermore, standing waves can be represented as sum of incoming and outgoing waves.

$$\vec{F}_{\sigma\mu\nu}^{(1)}(r', \theta', \emptyset') = \frac{1}{2} \left(\vec{F}_{\sigma\mu\nu}^{(3)}(r', \theta', \emptyset') + \vec{F}_{\sigma\mu\nu}^{(4)}(r', \theta', \emptyset') \right) \tag{3.11}$$

Keeping this and by substituting equations in the reverse direction starting from (3.10) going to (3.7), vector wave functions in the transmitting antenna coordinate system are expressed in the probe coordinate system as

$$\begin{aligned} & \vec{F}_{smn}^{(3)}(r, \theta, \emptyset) \\ & = \frac{1}{2} \sum_{\sigma\mu\nu} e^{im\emptyset_0} \, d_{\mu m}^n(\theta_0) e^{i\mu\chi_0} C_{\sigma\mu\nu}^{sn(3)}(kA) \left(\vec{F}_{\sigma\mu\nu}^{(3)}(r', \theta', \emptyset') \right. \\ & \left. + \vec{F}_{\sigma\mu\nu}^{(4)}(r', \theta', \emptyset') \right) \end{aligned} \tag{3.12}$$

Since, vector wave functions are expressed in the primed coordinate system, by substituting this expression in equation (3.6), the electric field radiated by the AUT can be written in the primed coordinate system as

$$\begin{aligned} & \vec{E}(r, \theta, \emptyset) \\ & = \frac{k}{\sqrt{\eta}} \sum_{\substack{smn \\ \sigma\mu\nu}} \frac{1}{2} q_{smn} e^{im\emptyset_0} d_{\mu m}^n(\theta_0) e^{i\mu\chi_0} C_{\sigma\mu\nu}^{sn(3)}(kA) \left(\vec{F}_{\sigma\mu\nu}^{(3)}(r', \theta', \emptyset') \right. \\ & \left. + \vec{F}_{\sigma\mu\nu}^{(4)}(r', \theta', \emptyset') \right) \end{aligned} \tag{3.13}$$

As discussed at the beginning of this chapter; complex signal is received through probe in practical measurement. Hence, expression for the receiving signal in equation (3.5) that is derived in section 3.1 can be used. However, since the probe and load can be

assumed as perfectly matched, the reflection coefficient Γ_l in the equation is zero. Then, by omitting summation received signal (w) can be described as

$$w = Ra \tag{3.14}$$

where R is the probe receiving coefficient vector $R_{\sigma\mu\nu}$ and a is the vector of mode coefficients of the incoming signal $a_{\sigma\mu\nu}$ where

$$a_{\sigma\mu\nu} = \frac{1}{2}\sum_{smn} q_{smn}e^{im\emptyset_0}\, d_{\mu m}^n(\theta_0)e^{i\mu\chi_0}C_{\sigma\mu\nu}^{sn(3)}(kA) \tag{3.15}$$

Note also that incident modes are represented by the $\vec{F}_{\sigma\mu\nu}^{(4)}(r',\theta',\emptyset')$ vector wave functions and $a_{\sigma\mu\nu}$ are the complex amplitudes of these vector wave functions. Because reflected signals between the probe and the AUT is assumed negligible, as second assumption $a_{\sigma\mu\nu}$ are not changed by these reflections.

Finally by omitting subscript 0 from $(\chi_0, \theta_0, \emptyset_0)$ and substituting equation (3.15) into equation (3.14), the signal received by the probe can be written as

$$w(A,\chi,\theta,\emptyset) = \frac{1}{2}\sum_{\substack{smn \\ \sigma\mu\nu}} q_{smn}e^{im\emptyset}\, d_{\mu m}^n(\theta)e^{i\mu\chi}C_{\sigma\mu\nu}^{sn(3)}(kA)R_{\sigma\mu\nu} \tag{3.16}$$

Equation (3.16) is the desired transmission formula. In this equation, $d_{\mu m}^n(\theta)$ and $C_{\sigma\mu\nu}^{sn(3)}(kA)$ are calculated for a given θ and A by using the formulas given in Appendix A & B. Moreover, it can be expressed as in equation (3.18) by representing the probe response constant as

$$P_{s\mu n}(kA) = \frac{1}{2}\sum_{\sigma\nu} C_{\sigma\mu\nu}^{sn(3)}(kA)R_{\sigma\mu\nu} \tag{3.17}$$

$$w(A,\chi,\theta,\emptyset) = \sum_{\substack{smn \\ \mu}} q_{smn}e^{im\emptyset}\, d_{\mu m}^n(\theta)e^{i\mu\chi}P_{s\mu n}(kA) \tag{3.18}$$

19

$w(A, \chi, \theta, \emptyset)$ are the received signals that are obtained from the measurement. Only unknowns in the equation are q_{smn} wave coefficients of the AUT. An equation is obtained for every measurement point $(\chi_j, \theta_j, \emptyset_j)$. Measurement is taken at as many discrete points as required by the number of modes. Then, system of linear equations can be constituted and solved directly. However, there is another method which is used mostly in practical cases [17]. Briefly, using orthogonality of the functions on the left hand side of equation (3.15), for every discrete point $(\chi, \theta, \emptyset)$ transmission formula is brought to form in equation (4.13) and by solving these as shown in (4.15), transmission wave coefficients are found. This solution is described in the next section. After wave coefficients are found, parameters on the left hand side of equation are all known and can be calculated for desired points of $(\chi, \theta, \emptyset)$. Then signal at the given distance is found only by summation.

3.3. Solution of the Transmission Formula

Solution of the transmission formula to find the spherical wave coefficients can be implemented in three steps. Orthogonality of the exponential function, which is defined in equation (3.19), for (χ) and $(\emptyset)$ variables is used.

$$\int_0^{2\pi} e^{i(m-m')\emptyset} d\emptyset = 2\pi\delta_{mm'} \tag{3.19}$$

For (θ) variable, orthogonality of the rotation coefficient $d_{\mu m}^n(\theta)$, which is defined in equation (3.20), is employed.

$$\int_0^{\pi} d_{\mu m}^n(\theta) d_{\mu m}^{n'}(\theta) \sin\theta \, d\theta = \frac{2}{2n+1}\delta_{nn'} \tag{3.20}$$

3.3.1. Solution in chi (χ)

The transmission formula (3.18) can be written as

$$w(A, \chi, \theta, \emptyset) = \sum_{\mu=-\nu_{max}}^{\nu_{max}} w_\mu(A, \theta, \emptyset)e^{i\mu\chi} \qquad (3.21)$$

where ν_{max} is the truncation value for the probe which can be calculated using equation (4.1) as $\nu_{max} = kr_p + n_1$ where r_p is the radius of the probe minimum sphere. Then $w_\mu(A, \theta, \emptyset)$ in equation (3.21) is

$$w_\mu(A, \theta, \emptyset) = \sum_{s=1}^{2}\sum_{n=1}^{N}\sum_{m=-n}^{n} q_{smn}e^{im\emptyset}d_{\mu m}^{n}(\theta)P_{s\mu n}(kA) \qquad (3.22)$$

In equation (3.21), $w_\mu(A, \theta, \emptyset)$ are finite Fourier series coefficients of $w(A, \chi, \theta, \emptyset)$ in chi (χ). Equation (3.21) can be solved by multiplying both sides with $e^{-i\mu'\chi}$ and integrating from 0 to 2π with respect to (χ) and then using exponential orthogonality, which is given in (3.19), following result is obtained.

$$\int_{0}^{2\pi} w(A, \chi, \theta, \emptyset)e^{-i\mu'\chi}d\chi = \int_{0}^{2\pi}\sum_{\mu=-\nu_{max}}^{\nu_{max}} w_\mu(A, \theta, \emptyset)e^{i(\mu-\mu')\chi} \, d\chi$$
$$= 2\pi w_{\mu'}(A, \theta, \emptyset) \qquad (3.23)$$

Then substituting μ instead of μ' for convenience results

$$w_\mu(A, \theta, \emptyset) = \frac{1}{2\pi}\int_{0}^{2\pi} w(A, \chi, \theta, \emptyset)e^{-i\mu\chi}d\chi \qquad (3.24)$$

where $\mu = -\nu_{max}, \dots, 0, \dots, \nu_{max}$. Note that it has the same form as in (4.13) which $w_\mu(A, \theta, \emptyset)$ is the Fourier transform of the measured data $w(A, \chi, \theta, \emptyset)$. Hence, it can be found using Discrete Fourier Transformation.

$$w_\mu(A, \theta, \emptyset)|\mu = 0,1,\dots,\nu_{max}, -\nu_{max},\dots,-1$$
$$= IDFT\{w(A, j\Delta\chi, \theta, \emptyset)|j = 0,1,\dots,J_\chi - 1\} \qquad (3.25)$$

where J_χ is the number of sample points in χ.

3.3.2. Solution in phi ($\emptyset$)

The transmission formula in equation (3.22) can be written as

$$w_\mu(A, \theta, \emptyset) = \sum_{m=-n}^{n} w_{\mu m}(A, \theta)e^{im\emptyset} \tag{3.26}$$

where

$$w_{\mu m}(A, \theta) = \sum_{s=1}^{2} \sum_{\substack{n=|m| \\ (n \neq 0)}}^{N} q_{smn} d_{\mu m}^{n}(\theta) P_{s\mu n}(kA) \tag{3.27}$$

In equation (3.27), $w_{\mu m}(A, \theta)$ are finite Fourier series coefficients of $w_\mu(A, \theta, \emptyset)$ in phi ($\emptyset$). Thus, it can be solved by the same way which is employed for chi and following result is obtained.

$$w_{\mu m}(A, \theta) = \frac{1}{2\pi} \int_{0}^{2\pi} w_\mu(A, \theta, \emptyset)e^{-im\emptyset} d\emptyset \tag{3.28}$$

where $m = -n, \dots, 0, \dots, n$. Note that again it has the same form as in (4.13) which $w_{\mu m}(A, \theta)$ is the Fourier transform of the $w_\mu(A, \theta, \emptyset)$. Hence, it can be found using Discrete Fourier Transformation.

$$\begin{aligned} w_{\mu m}(A, \theta)\big| m = {} & 0, 1, \dots, N, -N, \dots, -1 \\ = {} & IDFT\{w_\mu(A, \theta, j\Delta\emptyset)\big| j = 0, 1, \dots, J_\emptyset - 1\} \end{aligned} \tag{3.29}$$

where $J_\emptyset$ is the number of sample points in $\emptyset$.

3.3.3. Solution in theta ($\boldsymbol{\theta}$)

The transmission formula in equation (3.27) can be written as

$$w_{\mu m}(A, \theta) = \sum_{\substack{n=|m| \\ (n \neq 0)}}^{N} w_{\mu m}^{n}(A) d_{\mu m}^{n}(\theta) \tag{3.30}$$

where

22

$$w_{\mu m}^{n}(A) = \sum_{s=1}^{2} q_{smn} P_{s\mu n}(kA) \tag{3.31}$$

In equation (3.30), $w_{\mu m}^{n}(A)$ are finite Fourier series coefficients of $w_{\mu m}(A, \theta)$ in theta (θ). Equation (3.30) can be solved by multiplying both sides with $d_{\mu m}^{n'}(\theta) \sin \theta$ and integrating from 0 to π with respect to (θ) and then using orthogonality of the rotation function, which is given in (3.20), following result is obtained.

$$w_{\mu m}^{n}(A) = \frac{2n+1}{2} \int_{0}^{\pi} w_{\mu m}(A, \theta) d_{\mu m}^{n}(\theta) \sin \theta \, d\theta \tag{3.32}$$

Rotation coefficient can be expressed as the finite Fourier series (3.33).

$$d_{\mu m}^{n}(\theta) = i^{\mu - m} \sum_{m'=-n}^{n} \Delta_{m'\mu}^{n} \Delta_{m'm}^{n} e^{-im'\theta} \tag{3.33}$$

where $\Delta_{m'\mu}^{n}$ and $\Delta_{m'm}^{n}$ are constants which are defined by (A.4). Now, $w_{\mu m}^{n}(A)$ can be determined by evaluating the integral from samples of $w_{\mu m}(A, \theta)$. However, interval of theta in $w_{\mu m}(A, \theta)$ is defined only from 0 to π. Even if integrand is not periodic with these samples, $w_{\mu m}(A, \theta)$ can be extended into $\pi < \theta < 2\pi$ as

$$\widetilde{w}_{\mu m}(A, \theta) = \begin{cases} w_{\mu m}(A, \theta), & 0 \le \theta \le \pi \\ w_{\mu m}(A, 2\pi - \theta), & \pi < \theta < 2\pi \quad \mu - m \; even \\ -w_{\mu m}(A, 2\pi - \theta), & \pi < \theta < 2\pi \quad \mu - m \; odd \end{cases} \tag{3.34}$$

Functions $\widetilde{w}_{\mu m}(A, \theta)$ and $d_{\mu m}^{n}(\theta)$ have same parity and $\sin \theta$ is odd function. Therefore, integration value is zero if it is evaluated from 0 to 2π by using $\widetilde{w}_{\mu m}(A, \theta)$ instead of $w_{\mu m}(A, \theta)$. Because of this and since $\widetilde{w}_{\mu m}(A, \theta)$ is periodic function of θ with 2π, it can be used in the integral by expanding into the finite Fourier series (3.35).

$$\widetilde{w}_{\mu m}(A, \theta) = \sum_{l=-N}^{N} b_{l}^{\mu m} e^{il\theta} \quad 0 \le \theta < 2\pi \tag{3.35}$$

Eventually, $w_{\mu m}^{n}(A)$ is evaluated by inserting (3.35) and (3.33) into (3.32) as

$$w_{\mu m}^n(A)$$

$$= \frac{2n+1}{2} \int_0^\pi \sum_{l=-N}^N b_l^{\mu m} e^{il\theta} \, i^{\mu-m} \sum_{m'=-n}^n \Delta_{m'\mu}^n \Delta_{m'm}^n e^{-im'\theta} \sin\theta \, d\theta \quad (3.36)$$

$$= \frac{2n+1}{2} i^{\mu-m} \sum_{l=-N}^N b_l^{\mu m} \sum_{m'=-n}^n \Delta_{m'\mu}^n \Delta_{m'm}^n \int_0^\pi e^{i(l-m')\theta} \sin\theta \, d\theta$$

The integral in (3.36) can be evaluated by using

$$\int_0^\pi e^{i(l-m')\theta} \sin\theta \, d\theta = \begin{cases} \pm i \dfrac{\pi}{2}, & (l-m') = \pm 1 \\ 0, & |l-m'| = 3,5,7 \ldots \\ \dfrac{2}{1-(l-m')^2} & |l-m'| = 0,2,4 \ldots \end{cases} \quad (3.37)$$

Hence, only unknowns in (3.36) are $b_l^{\mu m}$ which are the Fourier coefficients of $\widetilde{w}_{\mu m}(A,\theta)$. Then it can be found using Discrete Fourier Transformation (3.38).

$$b_l^{\mu m} \big| l = 0,1,\ldots,N,-N,\ldots,-1$$
$$= IDFT\{\widetilde{w}_{\mu m}(A,j\Delta\theta) \big| j = 0,1,\ldots,J_\theta - 1\} \quad (3.38)$$

where J_θ is the number of sample points in θ.

$w_{\mu m}^n(A)$ are found for indices n, m, μ. When equation (3.31) is expanded by remembering $q_{1mn} = a_{mn}$ and $q_{2mn} = b_{mn}$

$$w_{\mu m}^n(A) = a_{mn} P_{1\mu n}(kA) + b_{mn} P_{2\mu n}(kA) \quad (3.39)$$

There will be equations as much unknowns as in (3.39) with respect to mode indices n, m, μ. Then, wave coefficients can be determined by solving system of equations. Note that linearly polarized probe, which has only azimuthal mode with $\mu = \pm 1$, is generally used in practical measurements. Therefore, equation (3.39) reduces to two equations with two unknowns a_{mn} and b_{mn}.

$$w_{-1m}^n(A) = a_{mn} P_{1-1n}(kA) + b_{mn} P_{2-1n}(kA) \quad (3.40)$$

$$w_{1m}^n(A) = a_{mn} P_{11n}(kA) + b_{mn} P_{21n}(kA) \quad (3.41)$$

Consequently, equations (3.40) and (3.41) can be solved for each m, n pair to determine the wave coefficients.

CHAPTER 4

NUMERICAL CONSIDERATION OF THE EXPANSION AND MEASUREMENT

4.1. Truncation of Modes

Spherical wave functions have some properties with respect to distance (r). Dependence on the distance is due to the radial functions $z_n^{(c)}(kr)$ and $\frac{1}{r}\frac{d}{dr}\left\{rz_n^{(c)}(kr)\right\}$ in the spherical wave functions. These radial functions have cutoff properties, i.e., they decay rapidly for r larger than cutoff distance. Cutoff distance of these functions is approximately $\frac{n}{k}$. An antenna that can be enclosed by a minimum sphere of radius r_0 may in principle radiate infinitely many modes. However, modes with $n > kr_0$ are rapidly attenuated because of cutoff property of the radial functions. As a result, only modes with $n < kr_0$ have importance and field expressions can be truncated at a value $n = N$. In general, truncation value N can be defined by including accuracy factor n_1:

$$N = kr_0 + n_1 \tag{4.1}$$

For practical purposes, n_1 is usually taken as 10. Nevertheless, higher values can be taken to increase accuracy. Note that m takes values $0, 1, 2, \dots, n$. Consequently, truncation of modes n means also truncation of modes m. By using this formula, truncation of the n in the summation can be done.

As a final remark, Ludwig [19] worked on the truncation value of N. He computed the radiated power from the antenna with respect to n. It is found that more than 99.9 percent of the radiated power is contained by the modes with $n \leq kr_0$. Works on the truncation of modes are also performed in this study and results are given in Chapter 5.

4.2. Numerical Integration Method

Any piecewise continuous and periodic function with 2π can be expressed by Fourier series expansion;

$$f(\emptyset) = \sum_{k=-\infty}^{\infty} c_k e^{jk\emptyset} \tag{4.2}$$

where coefficients c_k are computed as

$$c_k = \frac{1}{2\pi} \int_0^{2\pi} f(\emptyset) e^{-jk\emptyset} d\emptyset, \qquad k = \ldots, -1, 0, 1 \ldots \tag{4.3}$$

In practice, only Q samples denoted by $f(l\Delta\emptyset)$, $l = 0, 1, 2 \ldots, Q-1$ with $\Delta\emptyset = 2\pi/Q$, are available and the requirement is to obtain Fourier series coefficients, c_k, from these samples. If $f(\emptyset)$ is strictly band limited, which means $c_k = 0$ for $|k| > N$, Fourier series contains only finite number of terms, i.e.,

$$f(\emptyset) = \sum_{k=-N}^{N} c_k e^{jk\emptyset} \tag{4.4}$$

If $f(\emptyset)$ is not strictly band limited but terms with $|k| \leq N$ are dominant, truncated series in equation (4.4) becomes an approximation.

$$f(\emptyset) = \sum_{k=-\infty}^{\infty} c_k e^{jk\emptyset} \cong \sum_{k=-N}^{N} c_k e^{jk\emptyset} \tag{4.5}$$

By inserting sample points instead of $\emptyset$,

$$f(l\Delta\emptyset) = \sum_{k=-\infty}^{\infty} c_k e^{jkl\Delta\emptyset}, \qquad l = 0, 1, \ldots, Q-1 \tag{4.6}$$

k in equation (4.6) can be written as,

$$k = n + rQ, \qquad n = 0, 1, \ldots, Q-1, \qquad r = \cdots, -1, 0, 1 \ldots \tag{4.7}$$

28

Rearranging the infinite sum in equation (4.6) in groups of Q consecutive terms using indexing scheme in (4.7) yields,

$$f(l\Delta\emptyset) = \sum_{n=0}^{Q-1}\sum_{r=-\infty}^{\infty} c_{n+rQ}\, e^{j(n+rQ)l\Delta\emptyset}, \qquad l = 0,1,\dots,Q-1 \qquad (4.8)$$

Since $\Delta\emptyset = 2\pi/Q$, $e^{j(rQ)l\Delta\emptyset} = e^{j(rQ)l\frac{2\pi}{Q}} = 1$, equation (4.8) reduces to,

$$f(l\Delta\emptyset) = \sum_{n=0}^{Q-1} e^{jnl\Delta\emptyset}\sum_{r=-\infty}^{\infty} c_{n+rQ}, \qquad l = 0,1,\dots,Q-1 \qquad (4.9)$$

Defining aliased coefficient $\bar{c}_n$ as

$$\bar{c}_n = \sum_{r=-\infty}^{\infty} c_{n+rQ}, \qquad n = 0,1,\dots,Q-1 \qquad (4.10)$$

the samples of $f(\emptyset)$ can be expressed as

$$f(l\Delta\emptyset) = \sum_{n=0}^{Q-1} \bar{c}_n e^{jnl\Delta\emptyset}, \qquad l = 0,1,\dots,Q-1 \qquad (4.11)$$

Equation (4.11) is a set of Q linear equations at Q sample points for the Q unknowns $\bar{c}_n$. Actually, equation (4.11) is nothing but DFT and the coefficients $\bar{c}_n$ are solved by using inverse DFT instead of solving the system of equations, i.e.,

$$\bar{c}_n = \frac{1}{Q}\sum_{n=0}^{Q-1} f(l\Delta\emptyset)e^{-jnl\Delta\emptyset}, \qquad l = 0,1,\dots,Q-1 \qquad (4.12)$$

Since c_k is small for $|k| > N$, we may assume that $c_k \cong \bar{c}_n$ for $|k| \le N$ and $c_k \cong 0$ for $|k| > N$ if we choose a value $Q > 2N$.

Now, consider the following integral;

$$I_m = \frac{1}{2\pi}\int_0^{2\pi} f(\emptyset)\, e^{-jm\emptyset}d\emptyset, \qquad m = -N,\dots,0,\dots,N \qquad (4.13)$$

29

For quasi-band limited $f(\emptyset)$, the integral has the same form as the integral in equation (4.3). Therefore, a very good approximation can be obtained using (4.12), that is:

$$I_m \cong \frac{1}{Q} \sum_{l=0}^{Q-1} f(l\Delta\emptyset)e^{-jml\Delta\emptyset}, \qquad m = -N, ..., 0, ..., N \qquad (4.14)$$

where $Q = 2\pi/\Delta\emptyset$. If trapezoidal rule with equal weights at all sample points is applied to the integral in (4.13), we also get equation (4.14). However, considering equation (4.14) as the inverse DFT operator is much more useful since the FFT algorithm can be applied resulting in much less computational load, [17].

$$\{I_0, I_1, ..., I_N, , I_{-N}, ..., I_{-1}\} = IDFT\{f(l\Delta\emptyset)|l = 0,1, ..., Q - 1\} \qquad (4.15)$$

CHAPTER 5

APPLICATIONS AND RESULTS

Computation of far field pattern from the near field data without probe correction is described in Chapter 2. In this chapter, we first discuss the verification of this method. For this purpose, known field expression of a z directed Hertz Dipole located at the origin is used. In addition; different configurations have been tested by using coordinate rotation and translation of the Hertz Dipole. Furthermore; different numerical integration techniques have been used for calculation of these fields. Results and comparisons of them are discussed in this chapter. Finally; algorithm for the probe corrected case that is explained in Chapter 3 is tested. Using real antennas near field measurement data and probe receiving coefficients, far field patterns are obtained.

5.1. Near Field to Far Field Transformation for the Hertz Dipole

Hertz Dipole is an infinitesimal antenna excited by uniformly distributed current. Field distribution of Hertz dipole for any distance can be found easily. Hence; as a first step of verification of the transformation formula, field expression of the Hertz dipole is used. For the antenna shown in Figure 5.1, length l, which is much smaller than wavelength, carrying a current I_0, oriented along the z axis and located at the origin, fields expressions can be found as in equation (5.1) and equation (5.2) [20].
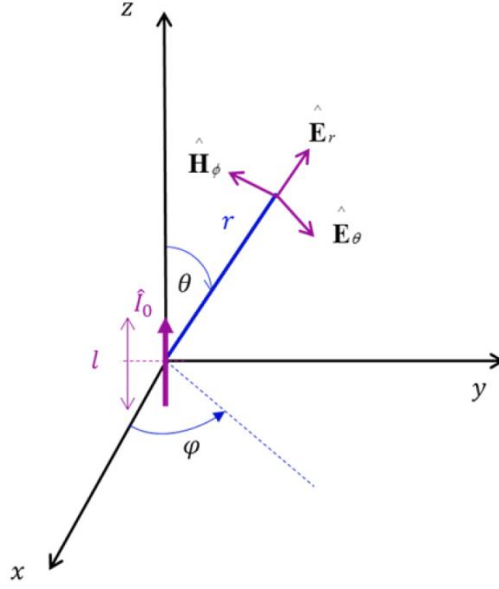
Figure 5.1. z-oriented Hertz Dipole placed at the origin [21]

$$\vec{E} = \left(1 - \frac{1}{ikr}\right)\left(\frac{\eta I_0 l e^{ikr}}{2\pi r^2}\cos\theta\right)\hat{r}$$
$$+ \left(1 - \frac{1}{ikr} - \frac{1}{(kr)^2}\right)\left(\frac{-i\eta k I_0 l e^{ikr}}{4\pi r}\sin\theta\right)\hat{\theta} \tag{5.1}$$

$$\vec{H} = \left(1 - \frac{1}{ikr}\right)\left(\frac{-ik I_0 l e^{ikr}}{4\pi r}\sin\theta\right)\widehat{\emptyset} \tag{5.2}$$

For $f = 3$ GHz, $I_0 = 1$ A, $l = 0.001$ m, which corresponds to much smaller value than the wavelength (0.1 m), and $r = 1$ m, electric field expression can be computed as if it is near field measurement result for discrete θ values. Then using these data, spherical wave expansion coefficients are computed as explained in Chapter 2. As can be understood from the field expressions in equation (5.1) and equation (5.2), Hertz dipole radiates only TM mode waves. In addition, since it is located at the origin, it has $\emptyset$ symmetry. Hence, it is expected to have just values for $m = 0$. Furthermore; Hertz dipole is infinitesimal antenna and because of this, its field expression has only

32

mode with $n = 1$. Therefore, only expected wave coefficient is b_{01} and others must be zero.

Results are shown in Table 5.1 and Table 5.2. As expected; apart from b_{01}, coefficients are almost zero.

Table 5.1. *TE Mode Wave Coefficients of the Hertz Dipole*

a_{mn}	$n = 1$	$n = 2$
$m = -2$	0	$(-3.3 + j2.8)10^{-15}$
$m = -1$	$(-13.6 + j0.54)10^{-15}$	$(-0.25 + j2.9)10^{-16}$
$m = 0$	$(-0.4 - j10.9)10^{-18}$	$(-58 + j0.05)10^{-18}$
$m = 1$	$(-11 - j0.73)10^{-15}$	$(-0.9 - j26)10^{-17}$
$m = 2$	0	$(3.2 - j4.9)10^{-15}$

Table 5.2. *TM Mode Wave Coefficients of the Hertz Dipole*

b_{mn}	$n = 1$	$n = 2$
$m = -2$	0	$(1.94 + j85.1)10^{-18}$
$m = -1$	$(-36 - j6.1)10^{-17}$	$(0.23 - j52)10^{-16}$
$m = 0$	-242.396	$(1.37 + j5.82)10^{-16}$
$m = 1$	$(-3 - j1.13)10^{-17}$	$(-3.1 - j38.8)10^{-16}$
$m = 2$	0	$(-1.3 - j5.35)10^{-17}$

After finding wave coefficients, far field pattern can be found. Far field expression of the electric field is given in equation (5.3).

$$\vec{E} = \left(\frac{jk\eta I_0 l}{4\pi} \frac{e^{-jkr}}{r} \sin\theta \right) \hat{\theta} \qquad (5.3)$$

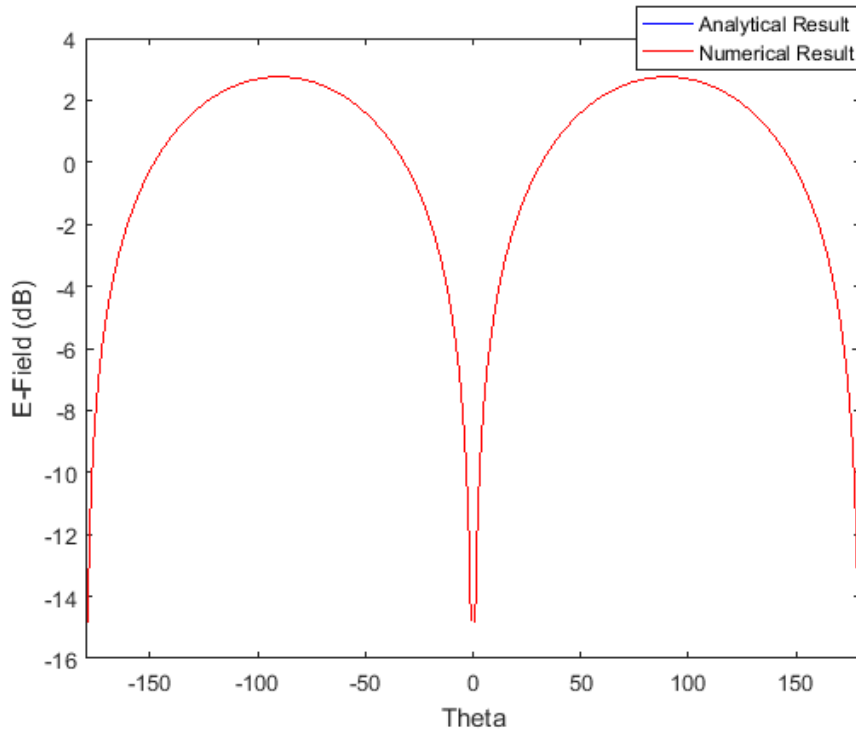By using expression directly and using wave coefficients, far field distributions are obtained (Figure 5.2).

Figure 5.2. Far Field Pattern of Hertz Dipole

As seen from Figure 5.2, far fields patterns are perfectly matched.

5.2. Near Field to Far Field Transformation for the Hertz Dipole with Rotation and Translation

In the previous section, wave coefficients for the *z* oriented Hertz dipole located at the origin are found and far field has been determined from these coefficients. For this configuration of the antenna, it is seen that the only nonzero coefficient is b_{01}. Hence, for numerical consideration and comparing the numerical integration techniques, it is better to have antenna which radiates more modes. In order to achieve this, some other type of antennas with analytically known field distribution can be used. Nevertheless; more flexible configuration can be established by rotation and translation of the Hertz Dipole. Field expressions of the Hertz Dipole can easily be modified for the rotation and translation. As a result, infinitely different radiation characteristics can be

34

obtained. Each of TE and TM or both with desired number of modes can be radiated. Therefore, transformation algorithm can be tested for lots of different cases.

Beside testing transformation algorithm, truncation number given by equation (4.1) is verified. Integrals, in equations (2.20) and (2.21), are solved using different numerical integration techniques. Results are examined and comparisons are made.

5.2.1. Tests for the Truncation Value

Transformation algorithm is tested by locating the Hertz Dipole described in section 5.1 along the z axis by distances $(delta_z)$ 0.05 m, 0.1 m and 0.2 m. For these cases, it is expected that only TM modes exist and $\emptyset$ symmetry of the radiation are protected. Therefore, only values for $m = 0$ are expected. However, since the antenna is moved along the z axis, more n modes are radiated. Radius of the smallest sphere enclosing all the sources can be taken as translation value $(r_0 = delta_z)$. Then, truncation value can be obtained using equation (4.1).

For the frequency $f = 3$ GHz, $k = 62.8$ and setting n_1 in equation (4.1) for the desired accuracy, following truncation values (N) are obtained.

Table 5.3. *Truncation Values Obtained for the Translations*

Translation Distance $(delta_z)$	Accuracy Factor (n_1)	Truncation Value (N)
0.05	2	6
0.1	3	10
0.2	3	16
0.3	4	23

Percentages of the total radiated power of modes are shown in Figure 5.3.
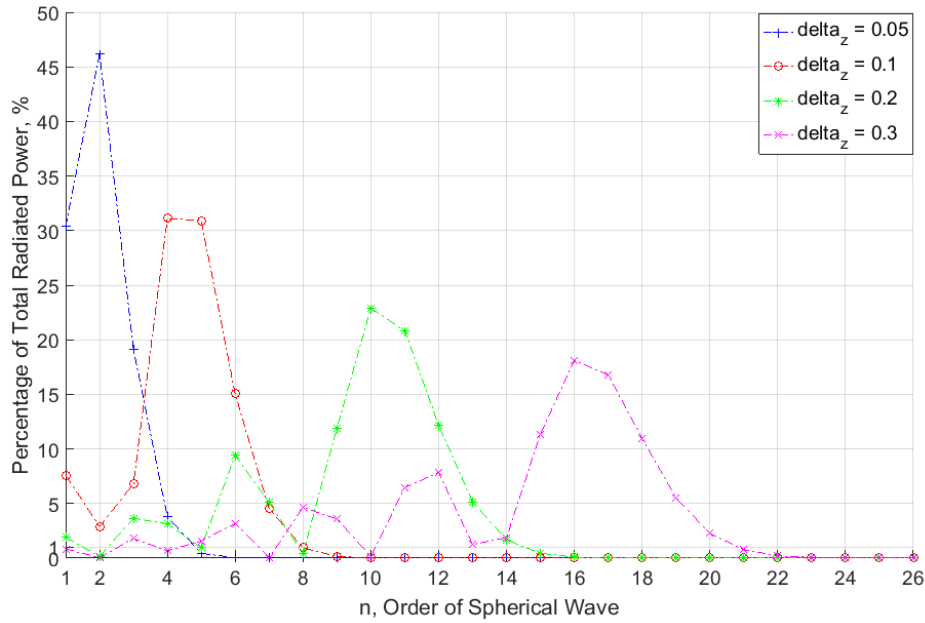
Figure 5.3. Percentage of Total Radiated Power with respect to n

As translation value is increased, radius of minimum sphere, that encloses all the sources, also increases. As a result, more modes are radiated and it can be seen clearly in Figure 5.3. It is also apparent that radiated powers are almost zero for the modes higher than the truncation values given in Table 5.3. Consequently, transformation algorithm and truncation value calculation in equation (4.1) are verified for these test cases.

5.2.2. Test for Numerical Integration Methods

In chapter 2, determination of the far field pattern from near field data is described. The most important calculation step in this method is finding the spherical wave coefficients which are given by equations (2.20) and (2.21). All functions in these equations are well defined. The only question arises in the calculation of the double integration. The first thing that comes to mind is to evaluate the integrals analytically. To do this, the electric field must be defined analytically. However, this does not apply to most practical cases. Measurements are taken at discrete points. Therefore, the solutions of these integrals can only be made numerically. There are lots of numerical

integration methods. However, there are advantages and disadvantages to each of them so deciding which method is the most efficient for our equation is important. First requirement from the method is being accurate and if possible exact. Other requirement is providing maximum accuracy with minimum number of data which is θ and $\emptyset$ sample points for our case. In addition; number of function evaluations, which will correspond to the calculation time, should be kept at minimum. One of the most well-known numerical integration methods is Gauss Quadrature rule, for which by using N sample points, can compute integrals of polynomial of degrees $2N - 1$ or lower exactly [22]. However, sample points in Gauss Quadrature are fixed. They are irrational numbers and not equally spaced. Thus; adjusting probe accurately to these sample points is not possible. Nevertheless, this method can be used for the near field data obtained theoretically and efficiency can be compared with other methods. Newton Cotes Rules are also well-known and commonly used integration techniques. In these rules, integrand is approximated as Lagrange polynomial and evaluation of this polynomial is performed. As the degree of polynomial increases, integration methods take different names as Trapezoidal Rule, Simpson's 1/3 Rule, Simpson's 3/8 rule, Boole's Rule, etc. Normally one can expect that as higher order polynomial is used, accuracy is increased. However, it is not always the case. As polynomial degree increases, oscillations at the edges of intervals arise and it may lead to very high degradation in the accuracy. Instead, using low order approximation rules with dividing intervals into subintervals is very efficient method and it is known as composite rule. In composite rules, integrand in the given interval is divided into small pieces and approximation is applied for every subinterval. By this way, accuracy can be increased by using more sample points. Finally, adaptive quadrature techniques or methods such as Romberg integration violate the last expectation. When they are used, accuracy can be increased but in turn more function evaluations for the calculations are added and extra sample points may be required in the measurement. Therefore; to increase accuracy by keeping calculation steps and time at minimum, Composite Newton Cotes Rules with more sample points can be used instead of using these methods. In addition; Gaussian Quadrature, namely Gaussian Legendre Rule can be

used for theoretical works. These rules are implemented and results and comparisons are discussed in this part. Also note that θ and $\emptyset$ integrations are not evaluated separately, instead double integration has been used.

As application, the configuration of the Hertz dipole given in section 5.2.1 with translation 0.1 m along z axis is used. It was explained and observed that all the coefficients are zero except b_{0n}. Furthermore, for 0.1 m translation, truncation value of $N = 10$ is obtained and verified experimentally. When equations (2.20) and (2.21) are considered, the functions $\vec{M}_{-\mu\nu}^{(c)}$ and $\vec{N}_{-\mu\nu}^{(c)}$ are defined for $\nu = 1,2 \ldots N$ and $\mu = -N \ldots -1,0,1 \ldots N$. Hence; in the functions $\vec{M}_{-\mu\nu}^{(c)}$ and $\vec{N}_{-\mu\nu}^{(c)}$, there are $2N$ harmonics. Then, $\vec{E}(r_0, \theta, \emptyset)$ electric field in equations (2.20) and (2.21) also includes $2N$ harmonics. Overall integrands in these equations are multiplication of the electric field and vector wave functions so it includes $4N$ harmonics. Although these integrands are not purely polynomial, if they are thought as $4N$ degree polynomials, then using Gauss Quadrature with $2N + 1$ degree, exact result can be obtained. Since truncation value N is calculated as 10, sample points (quadrature points) with $2N + 1 = 21$ can be starting value for tests. Firstly, b_{0n} coefficients are found using Gauss Quadrature with sample points of 500 which result of coefficients converge with this sample point. Hence, they are called as b_{0n_exact}. Then, b_{0n} coefficients are found using Gauss Quadrature and first four Newton Cotes Rules with 21 sample points. Percentage of relative errors, which are defined as $\frac{|b_{0n} - b_{0n\_exact}|}{|b_{0n\_exact}|} \times 100$, are calculated with respect to n and results are plotted in Figure 5.4 and Figure 5.5 separately because the differences between errors are too much.
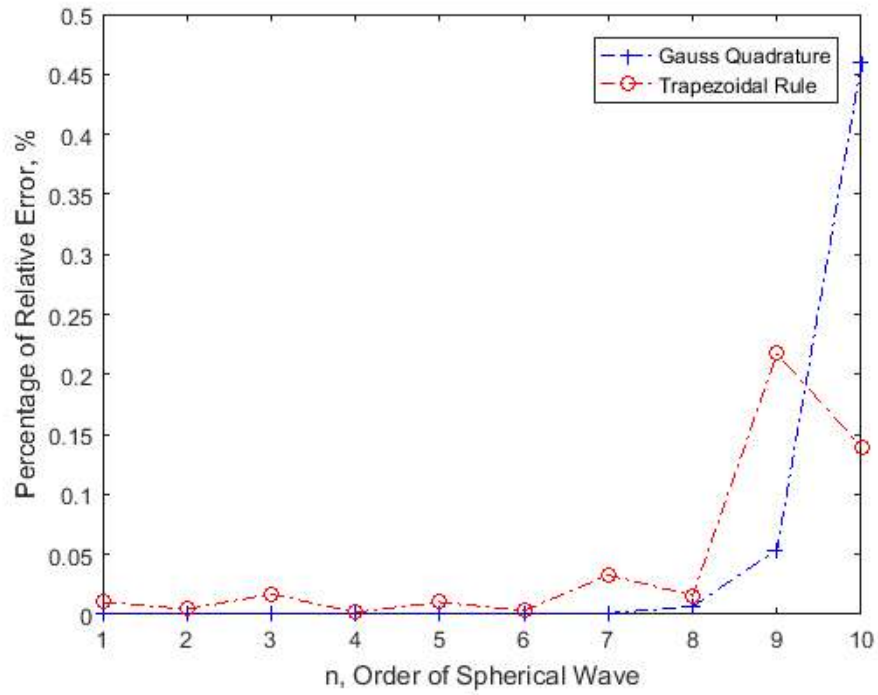
Figure 5.4 Comparison of Gauss Quadrature and Trapezoidal Rule for 21 Sample Points
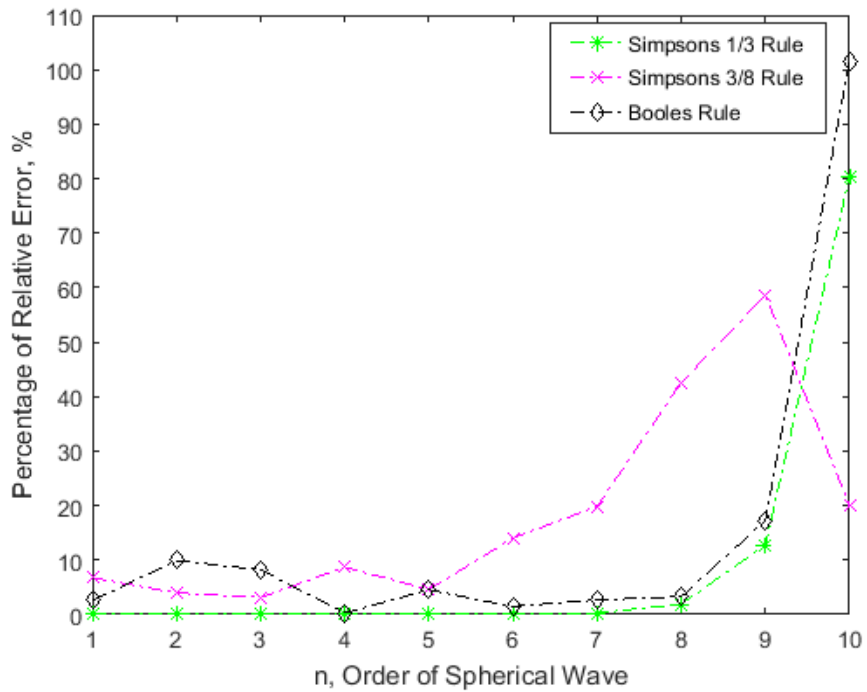

Figure 5.5 Comparison of Simpson's 1/3, 3/8 and Boole's Rule for 21 Sample Points

Figure 5.4 and Figure 5.5 show that Gauss Quadrature gives the least error. Although, accuracy of the Trapezoidal rule is smaller than Gauss Quadrature, they are very close. However, errors are quite high at this number of sample points for Simpson's 1/3, Simpson's 3/8 and Boole's rules.

Secondly, sample points (quadrature points) are increased and reductions in errors are observed. While doing this, convergence rate of the integration methods can also be examined. By increasing sample points sufficiently for every integration rule, errors are decreased approximately to 10^{-3}. Hence, required sample points for this error can be compared in Figure 5.6. Result of Boole's Rule is given in Figure 5.7 because this error cannot be reached even increasing sample points to 500.
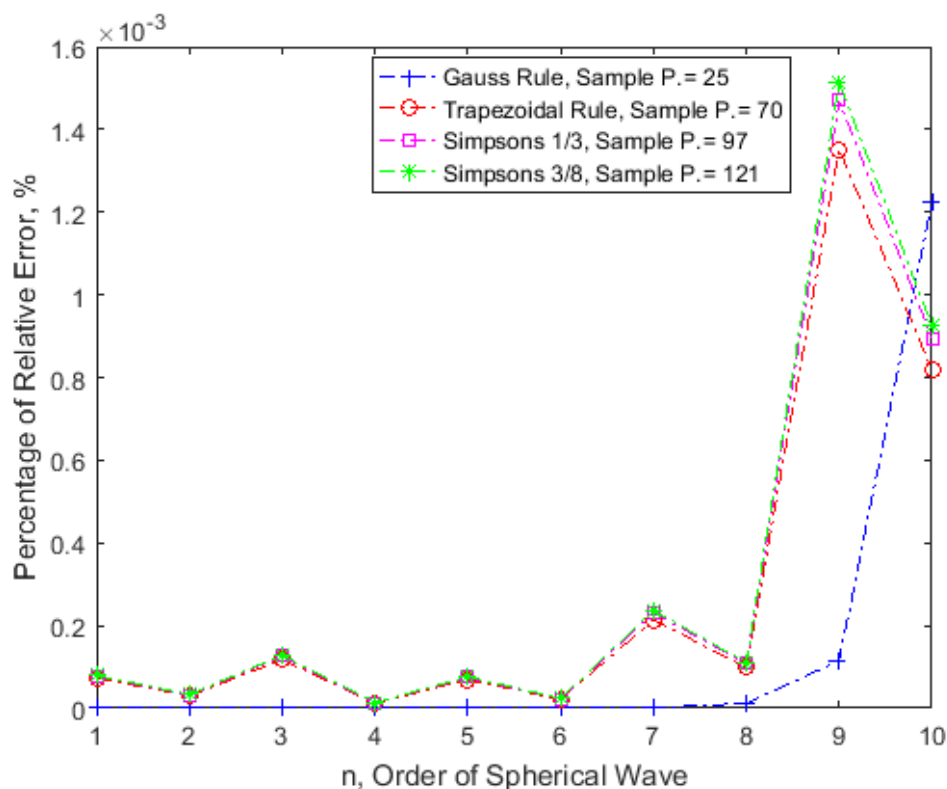

Figure 5.6 Comparison of Gauss, Trapezoidal and Simpson's 1/3 and Simpson's 3/8
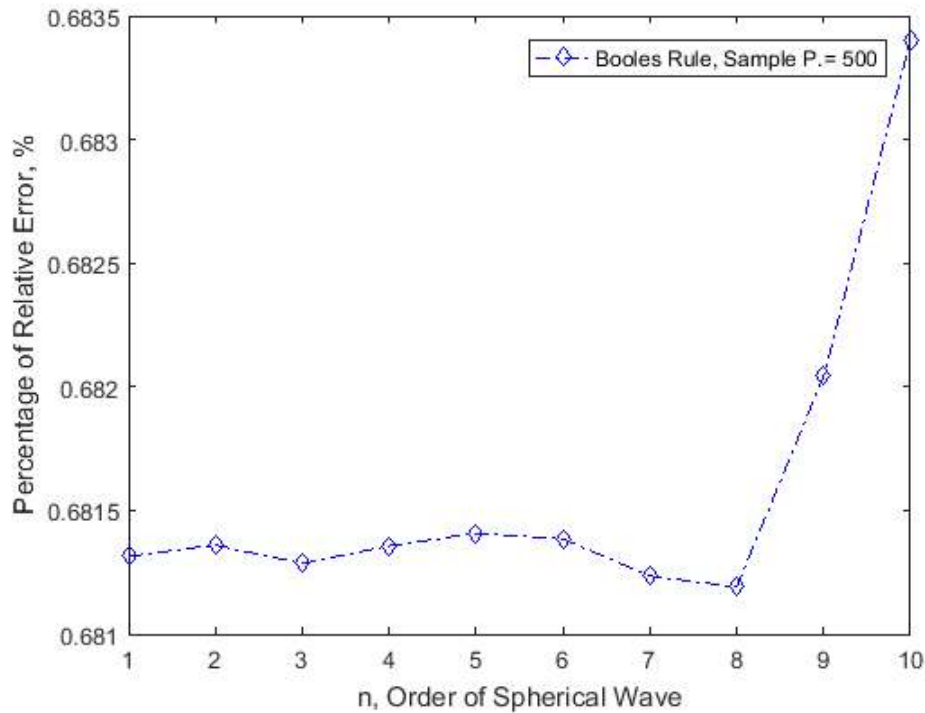
Figure 5.7 Boole's Rule with Sample Point of 500

First of all, results of Gauss Quadrature can be examined in Figure 5.4 and Figure 5.6. Percentage relative error is decreased approximately from 10^{-1} to 10^{-3} by just increasing sample point from 21 to 25. Required sample points to reach same error margin increases to 70 for Trapezoidal rule, 97 for Simpson's 1/3 rule and 121 for Simpson's 3/8 rule. As stated before increasing degree of approximating polynomial in the quadrature rule does not always provide more accuracy. Furthermore, it can be observed in Figure 5.7 that error is relatively high for Boole's rule. As a result, the integral expressions in transformation equations cannot be computed effectively with Boole's rule or the rule with higher order approximation polynomial. As mentioned previously, since sample points in Gauss Quadrature are irrational numbers and not equally spaced, it is not suitable for practical applications. Consequently; Trapezoidal rule provides the maximum accuracy with the minimum number of sample points. This is not surprising actually since it is found in section 4.2 that Trapezoidal rule gives exact result for the integral with periodic and band limited integrand. In addition;

41

considering inverse DFT operator same result is obtained with the Trapezoidal rule but using FFT algorithm results in much less computational load. Hence; FFT is used in the probe corrected algorithm. Results of them are given in the following section.

5.3. Near Field to Far Field Transformation from Measured Data

In this section, transformed far field patterns of the two antenna are investigated by using measured data of the antenna in the near field. The measurements of these antennas are performed in the spherical near field measurement set-up in the Department of Electrical and Electronics Engineering – Middle East Technical University (METU). The anechoic chamber was designed by ASYSOL which uses SNIFT algorithm by TICRA for the transformation. The far field patterns that are obtained from the developed algorithm with probe compensation in this work are compared to the patterns obtained TICRA's SNIFT transformation algorithm.

5.3.1. Results of the First AUT

Radius of the first AUT is 0.5 m and it is measured at frequency of 7.5 GHz. Probe distance is set to 3.12 m from the antenna origin. Wave number at this frequency is $k = \frac{2\pi}{\lambda} \cong 157.1$. If the radius of the minimum sphere surrounding the antenna is taken as radius of the antenna and omitting the accuracy factor, truncation value from equation (4.1) is found as 79. Sampling interval for this measurement was chosen as 2.5°. Then, truncation value N is equal to 72. After the near field data is obtained for these test parameters, far field transformation with TICRA (SNIFT) and algorithm developed in this study have been performed. For the ease of comparison, instead of 3D plot, far field patterns for $\emptyset = 0°$ are given in Figure 5.8.
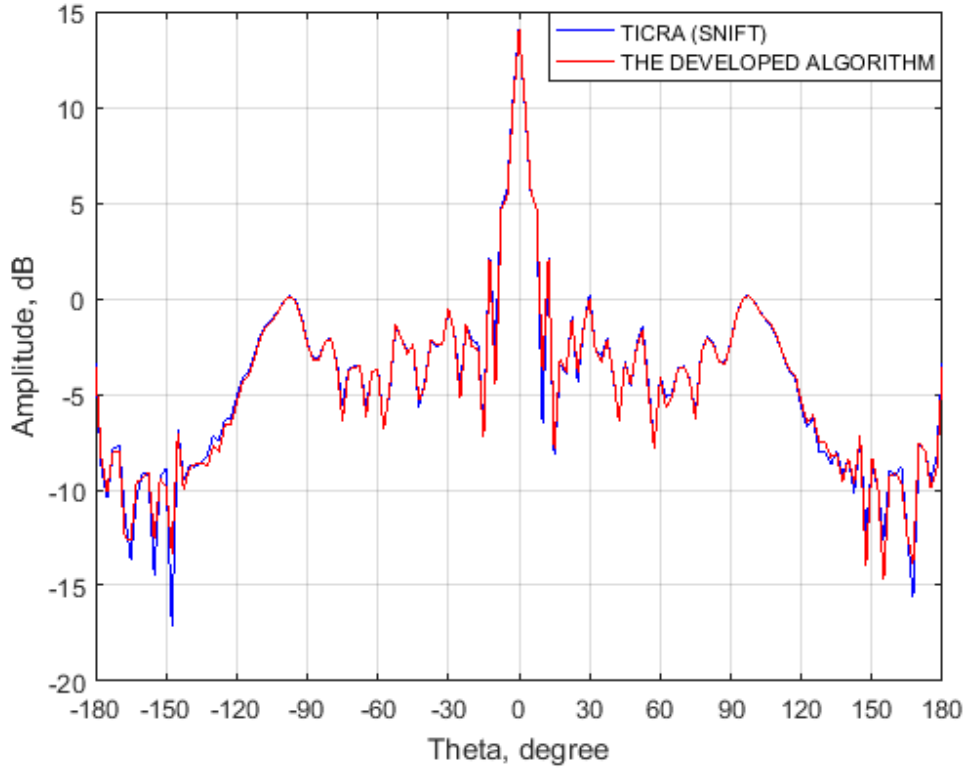
Figure 5.8. Far Field Pattern of First AUT

As can be seen from Figure 5.8, far field patterns are in a good agreement with each other. Furthermore, total radiated power (P) in watts can be found using wave coefficients as given in (5.4).

$$P = \frac{1}{2} \sum_{s=1}^{2} \sum_{n=1}^{N} \sum_{m=-n}^{n} |q_{smn}|^2 = \frac{1}{2} \sum_{n=1}^{N} \sum_{m=-n}^{n} |a_{mn}|^2 + |b_{mn}|^2 \qquad (5.4)$$

Then, radiated power for each mode of n can be defined as

$$P_n = \frac{1}{2} \sum_{m=-n}^{n} |a_{mn}|^2 + |b_{mn}|^2 \qquad (5.5)$$

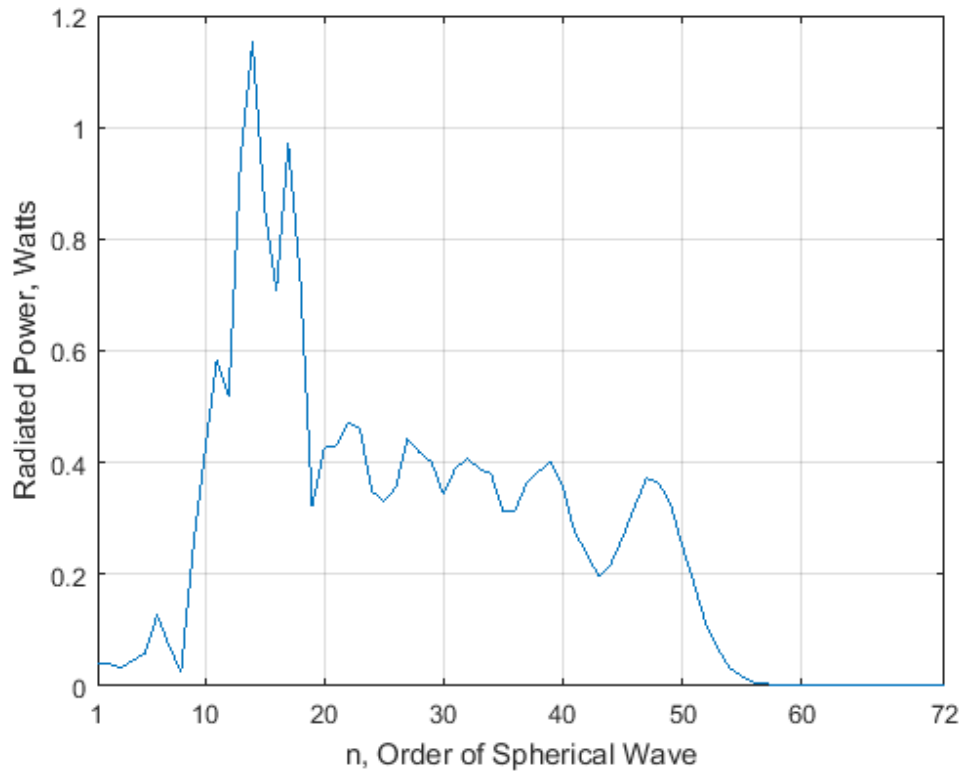P_n for the AUT is given with respect to n in Figure 5.9.

43

Figure 5.9. Radiated Power of First AUT with respect to n

Radiated power on the modes approaches to zero for n higher than 58. Truncation value for the AUT was calculated as 79 and by choosing sampling interval of 2.5°, value of n is truncated at 72. Therefore; as expected, almost all the radiated power is included using the truncation value formula. Studies have been done in the literature [19] and in this thesis show that the truncation formula works well. Nevertheless; it is recommended for each measurement to verify calculated value by observing the graph of radiated power with respect to n.

5.3.2. Results of Second AUT

Measured second AUT is smaller in size and operates at a higher frequency. The measurement frequency of the antenna is 12.7 GHz, radius is 0.315 m and measurement distance is taken as 2.5 m. Wave number at that frequency is $k \cong 266$. By taking the radius of the minimum sphere surrounding the antenna as radius of the

antenna and accuracy factor as $n_1 = 10$, truncation value from equation (4.1) is found as 94. When truncation number is selected as 100, sampling interval is set as $\frac{180°}{100} = 1.8°$. Note that if 94 is selected directly, numerical accuracy of the sampling interval is impaired ($\frac{180°}{94} = 1.91489\,...°$). However; sampling interval for this measurement is halved (0.9°) in order to increase accuracy. Therefore, transformation is performed up to $n = 200$. Far field patterns for $\emptyset = 0°$ can be seen in Figure 5.10.
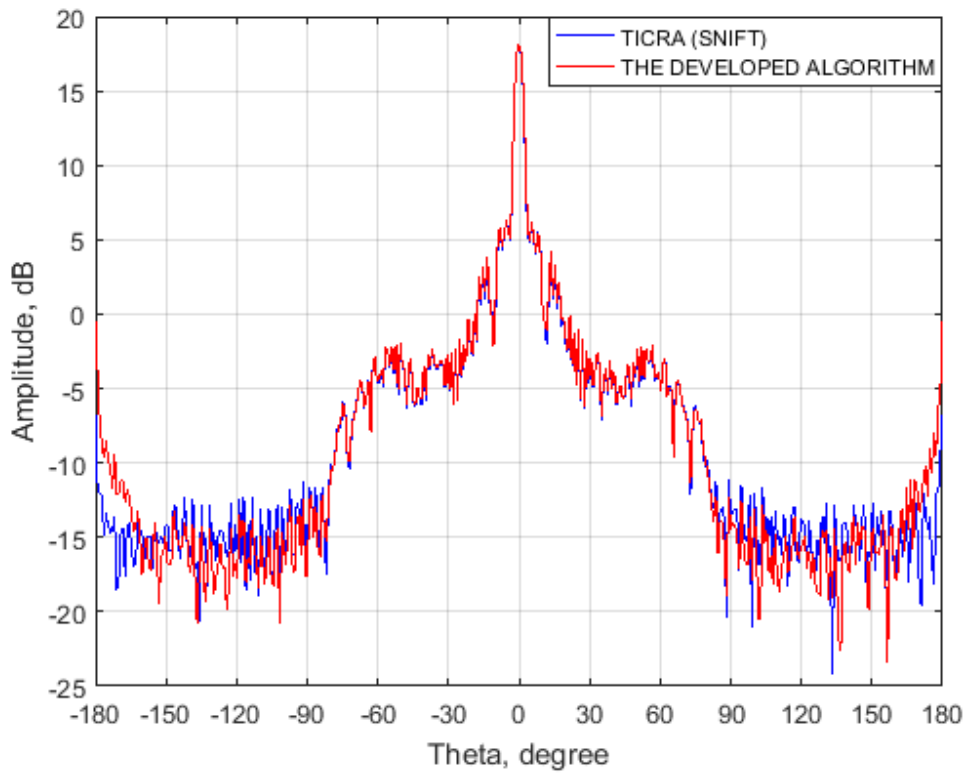

Figure 5.10. Far Field Pattern of Second AUT

It can be observed from Figure 5.10 that patterns are in a good agreement with each other except for some differences in the back lobes. Radiated power of the AUT for each mode of n is given in Figure 5.11.
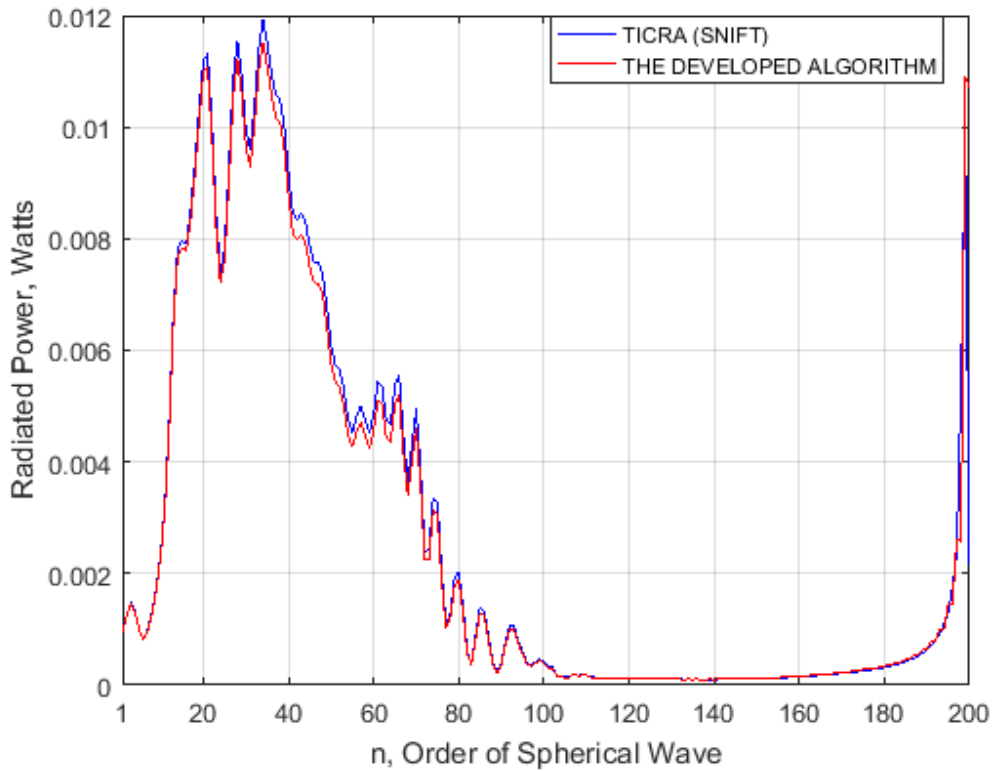
Figure 5.11. Radiated Power of Second AUT with respect to n

Results, which are given in Figure 5.11, are actually unexpected for n larger than approximately 150. It is also increasing sharply as approaching the truncation value. It is explained in section 4.1 that radiated power of an antenna must decay after some value of n. Hence; after the radiated power is decayed to zero nearly, increasing of it is not an expected situation. First, it comes to mind that numerical errors for high values of n may lead to this error. Remember that sampling interval is taken as 0.9° instead of 1.8° to increase accuracy. Transformation can be done by using same near field data with 1.8° sampling interval. Then, truncation value is set to 100 so calculation of higher values of n is discarded. Performing the transformation with these parameters results radiated power for each n as in Figure 5.12.
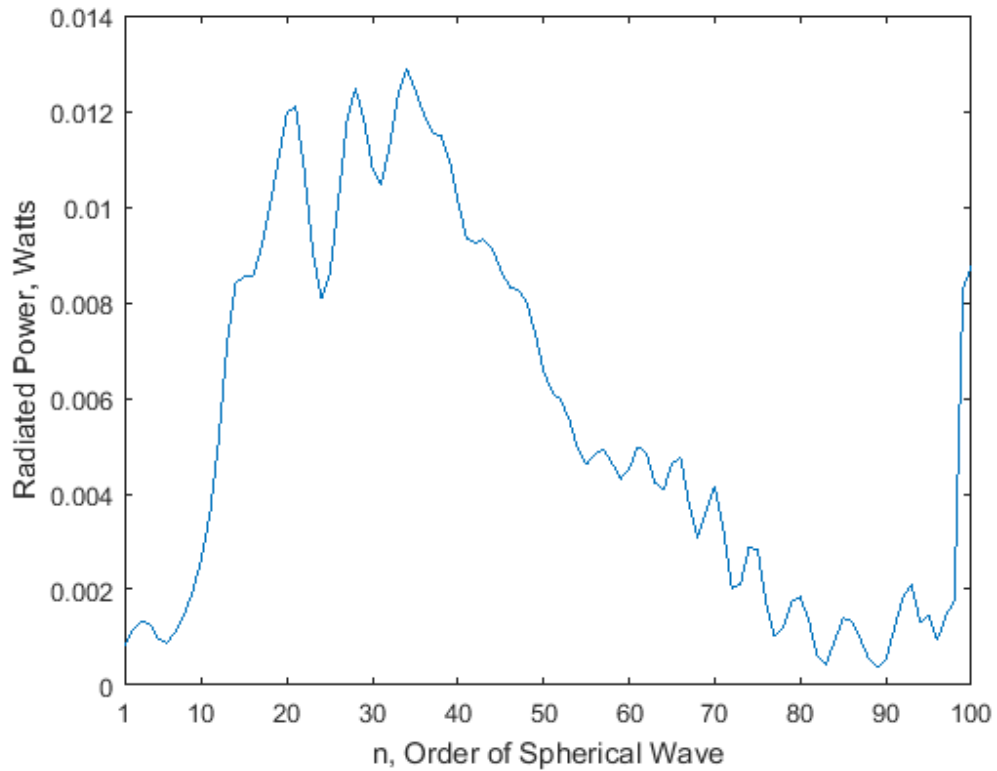
Figure 5.12 Radiated Power of Second AUT with respect to n

Again, there is same unexpected result. Hence, it is understood that high values of n does not lead to this error. Since error appeared for both cases, it may be originated from the measurement set-up or devices. Nevertheless, error analysis is performed to completely validate the algorithm in the following section.

5.4. Error Analysis

In order to investigate unexpected result of the second AUT and the limits of the algorithm, error analysis is done. Values of the rotation and translation coefficients in the transmission formula are calculated up to truncated value of n. In addition; recursion relations are used for the calculation of the rotation and translation coefficients as explained in Appendix A and Appendix B. Hence; analysis should be performed to observe whether an error arises when these are calculated for high values of n.

For the purpose of accurately analyzing this situation, near field data can theoretically be formed using equation (2.18). $\vec{M}_{mn}^{(c)}$ and $\vec{N}_{mn}^{(c)}$ are calculated for the specified m and n values. In addition, arbitrary values for the wave coefficients a_{mn} and b_{mn} can be taken. Thus near field data is established for any desired n modes and transformation of this fields to the far field is performed using the developed algorithm. Then, this far field data is the output of the algorithm and theoretical far field data is required to make comparison. It can be found by putting asymptotic form of the Hankel function in the vector wave functions of the equation (2.18). Radiated powers are also found from the wave coefficients. Then error in the radiated power with respect to n can be investigated. Tests has been done by increasing n from 1 to 500 and almost no error is observed. Order of the error for the radiated powers is nearly 10^{-13}. Some of them are given in Table 5.4.

Table 5.4. *Error in Radiation Power*

n	*Error*
100	10^{-14}
200	10^{-14}
300	10^{-13}
400	10^{-13}
500	10^{-13}

Theoretically calculated far field pattern and obtained far field pattern from the transformation algorithm for $n = 200$ are shown in Figure 5.13.
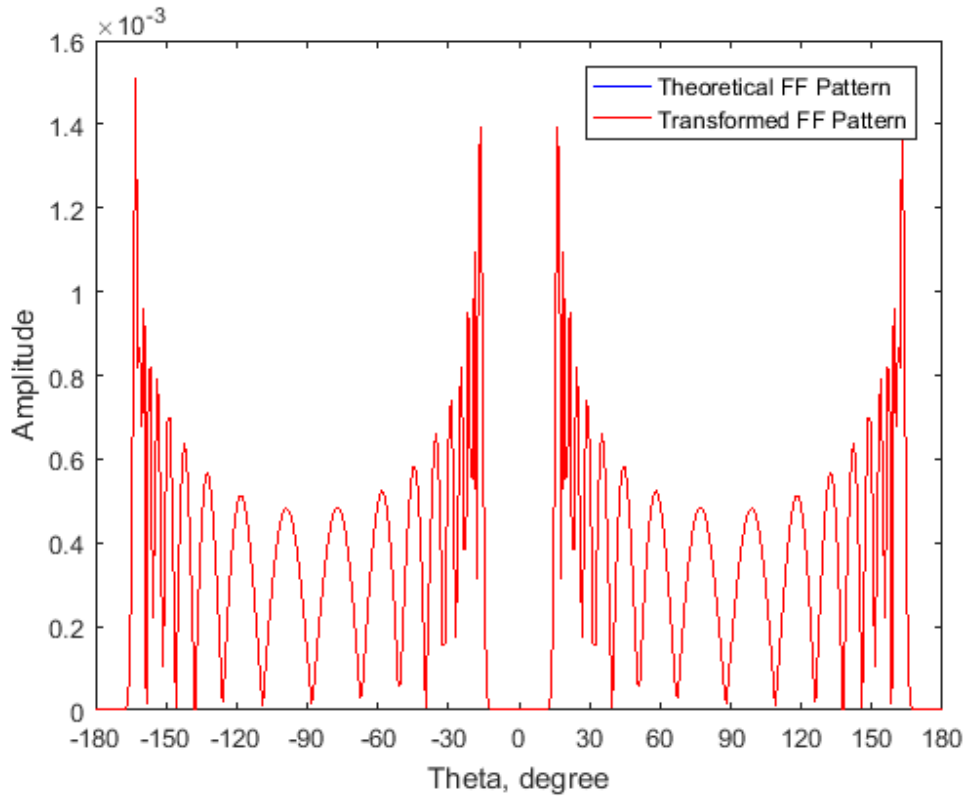

Figure 5.13. Theoretical and Transformed Far Field Patterns

It is observed that they are in full agreement. Note also that this analysis has been performed with lots of values of m and results are same. To sum up, algorithm is tested up to $n = 500$ and there is no error originated from the algorithm for the high values of n and m.

Remember that radiated power of the second AUT increased as closer to the truncation number. When the wave coefficients are examined, it is noticed that the powers of these high modes of n appears only at $m = \pm 1$. Then it comes mind that noises such as white noise can lead to these error terms. Therefore, error analysis is performed by adding white noise to the near field data. Error in the radiated power with respect to n and m is observed. In addition; theoretical and transformed far field patterns are

investigated. Percentage error of radiation power with respect to n for a specified m is shown in Figure 5.14. Percentage error of radiation power with respect to m for a specified n is also shown in Figure 5.15.
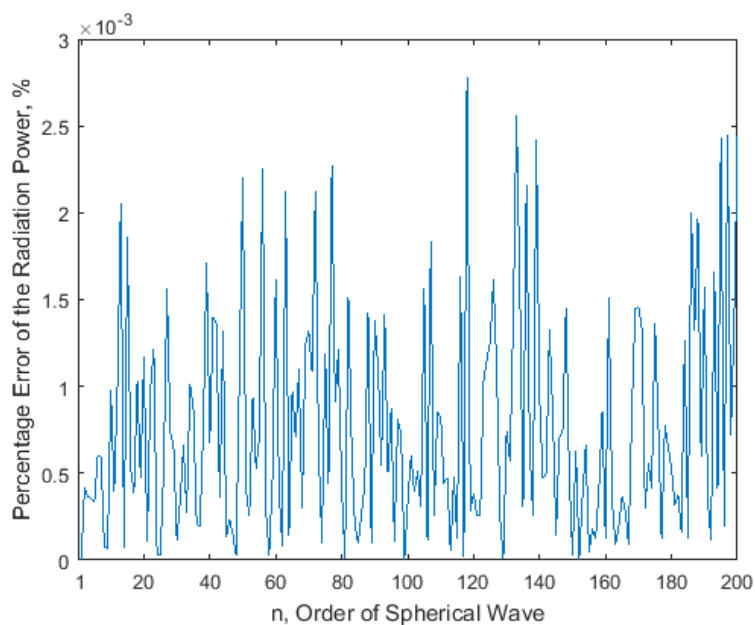

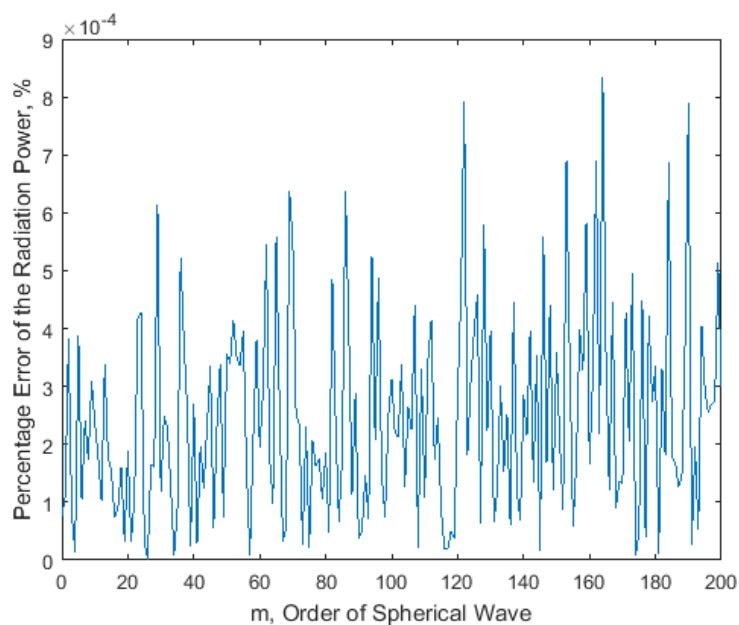*Figure 5.14.* Percentage Error of Radiation Power with White Noise

Figure 5.15. Percentage Error of Radiation Power with White Noise for n=200

50

Finally, theoretically calculated and transformed far field pattern for $n = 200$ and $m = 55$ can be seen in Figure 5.16.
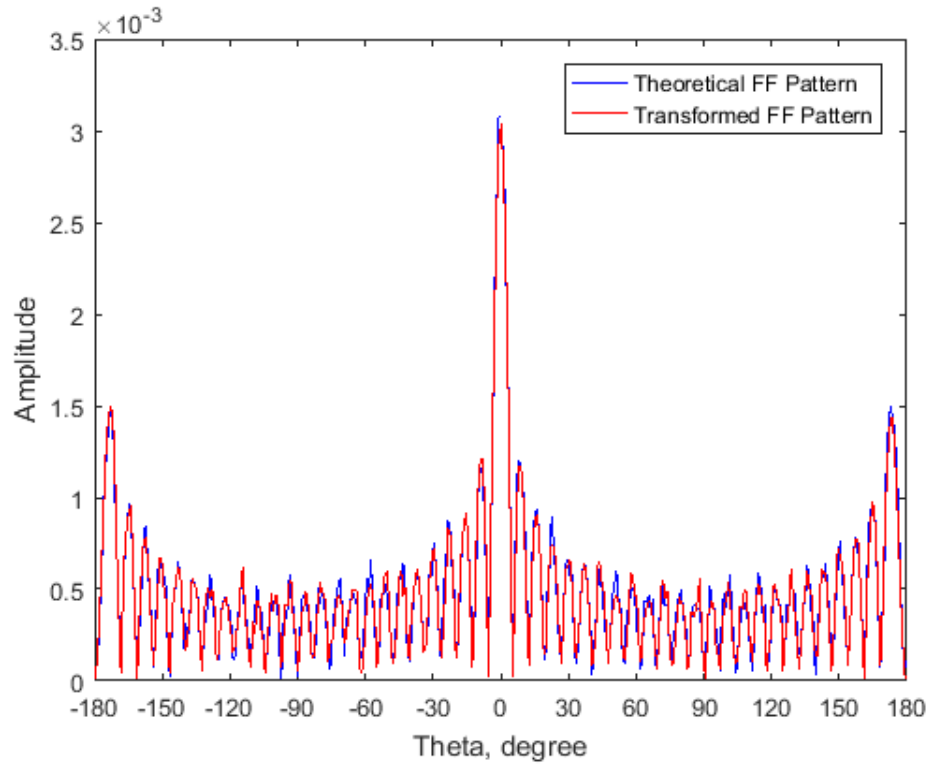

Figure 5.16. Theoretical and Transformed Far Field Patterns with White Noise

All the results with white noise are actually expected. It causes errors on each of n and m values on almost equal level. As a consequence of these errors, differences on the far field patterns are observed.

In conclusion, algorithm leads to no error for the high values of n and m. White noise have same grade of effect on all m and n values. Error in the radiated power of the second AUT appeared for both truncation values 100 (sampling interval 1.8°) and 200 (sampling interval 0.9°). However; same near field data is used for transformations. Hence, some mistake in the measurement setup or devices may have led to this error.

CHAPTER 6

CONCLUSIONS

In this thesis, spherical near field antenna measurement method is investigated. Vector solutions of the Maxwell's equations, which are called vector wave functions, are defined for the spherical coordinates. It is shown that any field can be expressed as the weighted sum of these vector wave functions. Finding weights or wave coefficients at the measurement distance allows us to obtain field at any other distance. Wave coefficients are found by taking advantage of orthogonality properties of the spherical wave functions. Then using these wave coefficients, electric or magnetic fields are found by summation. Even if this formulation is theoretically complete, in the practical antenna measurements, probe compensation should be done to obtain accurate results. Scattering matrix definition of the antenna is used to implement the probe compensation. The radiated field from the AUT is defined in the probe coordinate system by rotation and translation steps and including probe receiving coefficients, transmission formula with probe compensation is derived.

The field radiated from an antenna can only be defined by finite number of modes for the practical calculations. It is shown that there is a cut off value for spherical wave functions and modes higher than this are decayed exponentially. The value is dependent on order n. Formulation of the truncation value of n is given with respect to measurement frequency and radius of the antenna. The calculated values with this formulation are tested and results show that almost all the power radiated from the antenna is included.

Different numerical integration techniques are used in the calculations. As expected Gaussian Quadrature rule is the fastest converged technique but utilization of it in the antenna measurements is impractical because of irrational values of sample points

with unequal intervals. Among other techniques, trapezoidal rule gives the maximum accuracy with the minimum number of sample points. This is proved both theoretically and practically. In addition, it is shown that inverse DFT operator is much more useful than Trapezoidal rule since using the FFT algorithm results in much less computational load.

Eventually, measurement with two antennas are implemented and results are compared with TICRA's transformation algorithm (SNIFT). Good agreement in the results are obtained. Error analysis with respect to n and m are performed. It is observed that even very high values of n and m, which is tested up to 500, no error originated from the algorithm has been detected.

REFERENCES

[1] R. C. Johnson, H. A. Ecker, and J. S. Hollis, "Determination of far-field antenna patterns from near-field measurements," *Proc. IEEE*, vol. 61, no. 12, pp. 1668–1694, 1973.

[2] A. D. YAGHJIAN, "An overview of near-field antenna measurements," *IEEE Trans. Antennas Propag.*, vol. 34, pp. 30–45, 1986.

[3] M. H. Barnes and R. M. Barrett, "Automatic antenna wavefront plotter," *Electron.*, vol. 25, pp. 120–125, 1952.

[4] G. A. Woonton, "On the measurement of diffraction fields," *Proc. McGill Symp. Microw. Opt.*, pp. 347–350, 1953.

[5] T. E. Tice and J. H. Richmond, "Probes for Microwave Near-Field Measurements," *IRE Trans. Microw. Theory Tech.*, vol. 3, no. 3, pp. 32–34, 1955.

[6] J. H. Richmond, "Simplified Calculation of Antenna Patterns, with Application to Radome Problems," *IRE Trans. Microw. Theory Tech.*, vol. 3, no. 4, pp. 9–12, 1955.

[7] N. J. Gamara, "Pattern predictability on the basis of aperture phase and amplitude distribution measurements," *Electron. Def. Lab.*, 1960.

[8] E. V. Jull and J. Brown, "The prediction of aerial radiation patterns from near-field measurement," *Proc. Inst. Elec. Eng.*, vol. 108B, pp. 635–644, 1961.

[9] D. M. Kerns, "Analytical techniques for the correction of near-field antenna measurements made with an arbitrary but known measuring antenna," in *Abstracts of URSI-IRE Meeting*, 1963, pp. 6–7.

[10] W. Leach and D. Paris, "Probe compensated near-field measurements on a cylinder," *IEEE Trans. Antennas Propag.*, vol. 21, no. 4, pp. 435–445, 1973.

[11] F. Jensen, "Electromagnetic near-field far-field correlation," Tech. Univ. Denmark, 1970.

[12] P. F. Wacker, "Near-Field Antenna Measurements Using a Spherical Scan: Efficient Data Reduction with Probe Correction," *Inst. Elec. Eng. Conf. Publ. 113, Conf. Precis. Electromagn. Meas.*, pp. 286–288, 1974.

[13] P. F. Wacker, "Non-planar near-field measurements: Spherical scanning," *Electromagn. Div. Inst. Basic Stand. Natl. Bur. Stand. Boulder*, 1975.

[14] F. Jensen, "On the probe compensation for near-field measurements on a sphere," *Arch. Elektron. und Uebertragungstechnik*, vol. 29, pp. 305–308, Aug. 1975.

[15] F. H. Larsen, "Probe correction of spherical near-field measurements," *Electron. Lett.*, vol. 13, pp. 393–395, 1977.

[16] J. A. Stratton, *Electromagnetic Theory*. New York: McGraw-Hill, 1941.

[17] J. E. Hansen, *Spherical near-field antenna measurements*. The Institution of Engineering and Technology, London, United Kingdom, 1989.

[18] D. S. Jones, *The Theory of Electromagnetism*. Oxford, New York, Pergamon Press, 1964.

[19] A. C. Ludwig, "Near-Field Far-Field Transformations Using Spherical-Wave Expansions," *IEEE Trans. Antennas Propag.*, vol. 19, no. 2, pp. 214–220, 1971.

[20] C. A. Balanis, *Antenna theory*. John Wiley & Sons, Inc., Hoboken, New Jersey, 2005.

[21] B. Adamczyk, *Foundations of Electromagnetic Compatibility: with Practical Applications*. Wiley Publishing, 2017.

[22] E. Süli and D. F. Mayers, *An Introduction to Numerical Analysis*. Cambridge University Press, 2003.

[23] A. R. Edmonds, *Angular Momentum in Quantum Mechanics*. Princeton University Press, 1957.

APPENDICES

A. The Rotation Coefficient

The rotation coefficient $d_{\mu m}^n(\theta)$ is given by Edmonds [23] as

$$d_{\mu m}^n(\theta) = \left\{ \frac{(n+\mu)!\,(n-\mu)!}{(n+m)!\,(n-m)!} \right\}^{\frac{1}{2}} \sum_\sigma \binom{n+m}{n-\mu-\sigma}\binom{n-m}{\sigma}$$
$$(-1)^{n-\mu-\sigma}\left(\cos\frac{\theta}{2}\right)^{2\sigma+\mu+m}\left(\sin\frac{\theta}{2}\right)^{2n-2\sigma-\mu-m} \tag{A.1}$$

where the symbol

$$\binom{i}{j} = \frac{i!}{(i-j)!\,j!} \tag{A.2}$$

is the binomial coefficient. σ includes the terms that binomial coefficients do not lead to negative values for the factorials.

The finite Fourier series expansion of the rotation coefficient is given in equation (A.3).

$$d_{\mu m}^n(\theta) = i^{\mu - m} \sum_{m'=-n}^{n} \Delta_{m'\mu}^n \Delta_{m'm}^n e^{-im'\theta} \tag{A.3}$$

where delta function $\Delta_{m'm}^n$ is defined as

$$\Delta_{m'm}^n = d_{m'm}^n\left(\frac{\pi}{2}\right) \tag{A.4}$$

Delta functions can be found from two recurrence relations given in equations (A.5) and (A.6).

$$\sqrt{(n+m'+1)(n-m')}\Delta_{m'+1,m}^n$$
$$+ \sqrt{(n-m'+1)(n+m')}\Delta_{m'-1,m}^n + 2m\Delta_{m'm}^n = 0 \tag{A.5}$$

$$\sqrt{(n+m+1)(n-m)}\Delta^n_{m',m+1}$$
$$+\sqrt{(n-m+1)(n+m)}\Delta^n_{m',m-1} - 2m'\Delta^n_{m'm} = 0 \quad \text{(A.6)}$$

B. The Translation Coefficient

Translation coefficients for $kA > 0$ can be computed as:

$$C^{sn(c)}_{\sigma\mu\nu}(kA) = \sqrt{\frac{(2n+1)(2\nu+1)}{n(n+1)(\nu+1)}}\sqrt{\frac{(\nu+\mu)!\,(n-\mu)!}{(\nu-\mu)!\,(n+\mu)!}}(-1)^\mu$$
$$\frac{1}{2}i^{(n-\nu)}\sum_{p=|n-\nu|}^{n+\nu}[i^{-p}(\delta_{s\sigma}\{n(n+1)+\nu(\nu+1)-p(p+1)\}$$
$$+\delta_{3-s,\sigma}\{2i\mu kA\})a(\mu,n,-\mu,\nu,p)z^{(c)}_p(kA)] \quad \text{(B.1)}$$

where $a(\mu,n,-\mu,\nu,p)$ is a so called linearization coefficient and can be written in terms of the Wigner $3-j$ symbols

$$a(\mu,n,-\mu,\nu,p) = (2p+1)\left\{\frac{(n+\mu)!\,(\nu-\mu)!}{(n-\mu)!\,(\nu+\mu)!}\right\}^{\frac{1}{2}}$$
$$\begin{pmatrix} n & \nu & p \\ 0 & 0 & 0 \end{pmatrix}\begin{pmatrix} n & \nu & p \\ \mu & -\mu & 0 \end{pmatrix}. \quad \text{(B.2)}$$

Instead of solving Wigner $3-j$, translation coefficients with $\mu = {}^+_-1$ are sufficient for most of the practical cases.

Then, translation coefficient with $\mu = +1, \nu \geq 1$

$$C_{\sigma 1 \nu}^{sn(c)}(kA) = \frac{1}{4} i^n \frac{\sqrt{2n+1}}{n(n+1)} i^{-\nu} \frac{\sqrt{2\nu+1}}{\nu(\nu+1)}$$

$$\sum_{p=|n-\nu|,2}^{n+\nu} \left[\left\{ \delta_{s\sigma} \frac{\left(n(n+1) + \nu(\nu+1) - p(p+1)\right)^2}{n+\nu+p+1} \right. \right.$$

$$\left. + \delta_{3-s,\sigma} 2ikA \frac{(n+1) + \nu(\nu+1) - p(p+1)}{n+\nu+p+1} \right\}$$

$$* \frac{\left(\dfrac{-n+\nu+p}{2}\right)\left(\dfrac{n-\nu+p}{2}\right)\left(\dfrac{n+\nu-p}{2}\right)}{\left(\dfrac{n+\nu+p}{2}\right)}$$

$$\left. * i^{-p}(2p+1)h_p^{(c)}(kA) \right] \qquad (B.3)$$

where $p = |n-\nu|, |n-\nu| + 2, \dots, n+\nu-2, n+\nu$.

Translation coefficient with $\mu = -1, \nu \geq 1$ can be found easily.

$$C_{\sigma,-1,\nu}^{sn(c)}(kA) = (-1)^{s+\sigma} C_{\sigma 1 \nu}^{sn(c)}(kA) \qquad (B.4)$$

In equation (B.3) the binomial coefficients are of the form

$$B(J) = \binom{J}{J/2} \qquad (B.5)$$

where J is an even integer. When these binomial coefficients are replaced by

$$B'(J) = \binom{J}{J/2} 2^{-J} \qquad (B.6)$$

Overall result of the four binomial coefficient in equation (B.3) does not change but numerically more convenient form is obtained and it can be solved by using recurrence

formula in equation (B.7).

$$B'(J + 2) = \frac{J + 1}{J + 2} B'(J)$$

(B.7)

with the initial value $B'(0) = 1$.